Porous Silicon as Host and Template Material for Fabricating Composites and Hybrid Materials

9

Eugene Chubenko, Sergey Redko, Alexey Dolgiy, Hanna Bandarenka, Sergey Prischepa, and Vitaly Bondarenko

CONTENTS

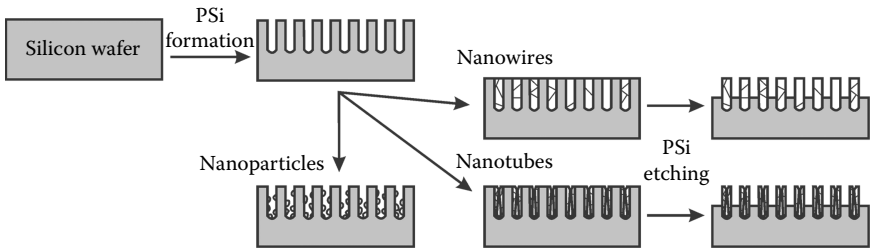

FIGURE 9.1 Formation of nanostructures with PSi template.

9.1 INTRODUCTION

The open porous structure and very large specific surface area of porous silicon (PSi) have driven scientists to introduce different foreign substances into its pores to fabricate PSi-based composite and hybrid materials (Hérino et al. 1997; Hérino 2000). Under this approach, PSi plays a role of host material, which receives foreign substances as "guests": metals, semiconductors, and carbon-containing materials (polymers, fullerenes, carbon nanotubes, and graphene). Nowadays in most cases, PSi is considered a template, that is, a type of host material with the structure that defines a shape of a "guest" substance. Elongated pores of PSi provide a formation of nanowires (NWs) and nanotubes (NTs) with high aspect ratio (more than 1:100) or formation of nanoparticles (NPs) at initial stages of the filling process. Process flow for fabrication of NWs, NTs, and NPs using PSi as template is shown schematically in Figure 9.1. The aims of filling of PSi pores are: (1) to obtain 1D nanostructures with high aspect ratio and anisotropy of properties; (2) to fabricate 1D and 0D structures showing unusual properties caused by quantum size effects; (3) to provide an electrical contact to the whole PSi surface; and (4) to integrate composite and hybrid materials with CMOS, MEMS, and NEMS devices. Composite material is a mixture of similar kinds of materials while hybrid consists of different kinds of materials (organic and inorganic) with chemical bonds between them. The main distinction between composite and hybrid is that the second one possesses properties, which do not exist in either of its parent components (Drisko and Sanchez 2012).

Deposition of guest substances in PSi can be carried out by vacuum-based methods such as thermal evaporation, magnetron sputtering, and chemical vapor deposition (CVD) or from the liquid phase, for example, the electrochemical and chemical deposition, sol-gel method. Most vacuum-based techniques provide the deposition of guest substance predominantly on the top of the PSi layer. Nevertheless, the optimization of CVD technologies provides readily filling pores of 20–120 nm in diameter excepting a blockade of pore entrances that earlier occurred because pore constrictions suppressed the depositing process. Atomic layer deposition (ALD) provides great scope even for filling the pores of thick meso-PSi (Grigoras et al. 2014). The advantage of the deposition from the liquid phase is low temperature as it prevents PSi sintering, which takes place at heating up to Tammant's temperature (572°C for Si) (Labunov et al. 1986), and easy infiltration of the pores with deposition medium defined by wettability and capillary effects contributing to filling pores with guest substance.

Chapter 9 is a review of recent research in the field of fabrication, properties, and applications of PSi-based composites and hybrid materials. For detailed information on the early research, it is advised to refer to the primary sources or reviews of Hérino et al. (1997) and Hérino (2000).

9.2 FORMATION, PROPERTIES, AND APPLICATIONS OF METAL/PSi COMPOSITES

For the formation of metal/PSi composites, the deposition from the liquid phase is more often used. Chemical reactions between PSi and deposited metals hardly ever occur providing distinct silicon/metal interface. Nevertheless, in some cases the formation of silicides is observed (Dolgiy et al. 2012a). The metal deposition from the liquid phase can be performed electrochemically

or without applying electric current (Zhang 2001; Ogata et al. 2006). Both processes are electrochemical by nature in that the deposition of metal atoms is a reduction reaction involving a charge transfer. In the electrochemical deposition method, electrons are delivered by electric current flowing through the electrolyte/substrate interface. The electrochemical method can provide uniform pore filling, especially when PSi skeleton is fully depleted, because in this case the current localization at the pore bottoms takes place. In the electroless deposition, electrons are provided either by a reducing agent or by the silicon substrate due to the corrosion processes. In the last case, the displacement of Si atoms with metal ions occurs. Only several metals (Cu, Hg, Ag, Pd, Pt, Au) that have the electrochemical potential higher than +0.187 V (the reduction potential of Si in HF-based solutions) can be deposited on bulk Si by the displacement process. Compared to bulk Si, the reduction of metals on PSi occurs more easily due to the presence of Si–H species on the pore walls and elemental silicon in the skeleton. The reduction potential of either of these species can reduce many metal ions not limited by those listed above down to their elemental state (Coulthard et al. 1993; Tsuboi et al. 1998; Parbukov et al. 2001; Harraz et al. 2002; Xu et al. 2007a,b). As for the electrochemical method, metals placed to the right of Al in the metal activity series can be deposited in PSi from the aqueous solutions. Other metals, in particular rare earth elements (REEs), tend to deposit in the form of hydroxides, forcing the use of nonaqueous solutions (Petrovich et al. 2000a,b). PSi doping with REEs by the electrodeposition method is described in Chapter 9, Section 9.7.2, in *Porous Silicon: Formation and Properties*.

9.2.1 FERROMAGNETIC METALS

Ni, Co, and Fe are the most interesting ferromagnetic metals to fabricate PSi-based composites. They have high Curie temperature (1043 K, 1403 K, and 631 K for Fe, Co, and Ni correspondingly), conditioning inherent magnetization in the wide temperature range. Other ferromagnetic metals can have high spontaneous magnetization (for example, 0.2713 T for Tb against 0.17352 T for Fe) but quite low Curie temperatures (223 K for Tb), so additional cooling is required to explore their magnetic properties. Magnetic NWs and NPs, grown in PSi, demonstrate magnetic anisotropy, giant magnetoresistance, and coherent spin waves. These properties are important for various magnetic applications such as magnetic recording, magneto-optics, sensor technology, and spintronics (Fert and Piraux 1999; O'Brien et al. 2009; Fernández-Pacheco et al. 2013)

The pioneering study into the Ni electrochemical deposition in PSi was directed to the formation of thick Ni silicides (Hérino et al. 1985). Uniform Ni deposition was achieved only for thin 0.5-μm PSi layer. The Ni silicides formation occurred after annealing in dry nitrogen. The idea of the thick silicide formation gained further progress in the works by Borisenko et al. (1989, 1990) where silicides based on electrodeposited Co were fabricated and studied. Uniaxial anisotropy of the magnetic properties of Ni NWs formed in PSi was first shown by Gusev et al. (1994). In this work, Ni was deposited electrochemically in the 30-μm thick meso-PSi layer in the potentiodynamic regime with the frequency of 50 Hz. It provided uniform filling of PSi with Ni along pores.

Recent Ni/PSi composites formation study is aimed to develop a reliable technology for the deposition of Ni in PSi with a high filling factor F_f, uniformity, and reproducibility. The research group of the University of Graz (Granitzer et al. 2005) electrochemically deposited Ni in PSi in the way described by Gusev et al. (1994). As a result, an irregular array of Ni NWs arranged with ~2.5×10^9 mm^{-2} surface density was formed. Lagging of magnetization M behind variations of the magnetic field, H (a hysteresis loop) was found by SQUID magnitometric study as a dependence $M(H)$ in the range of weak magnetic fields to be dependent on the field direction (in or out of plane). The Ni electrochemical deposition in a pulse mode with an alternation of direct and returning pulses improved pore filling with Ni that was deposited as nanostructures of varying size and shape (Rumpf et al. 2006). As shown in Figure 9.2, shape of the deposited Ni-nanostructures varied from spheres (which diameters were defined by the pore diameters) through ellipsoids to high aspect ratio needle-like structures by decreasing the pulse duration from 40 to 5 s (Granitzer and Rumpf 2010).

Hysteresis in the $M(H)$ dependence in the range of strong magnetic fields (~5 T) was found to depend on the size of NWs. Surface magnetism of giant orbital interaction was also observed. It led to paramagnetic effect in strong magnetic fields. The $M(H)$ curve behavior in the range of

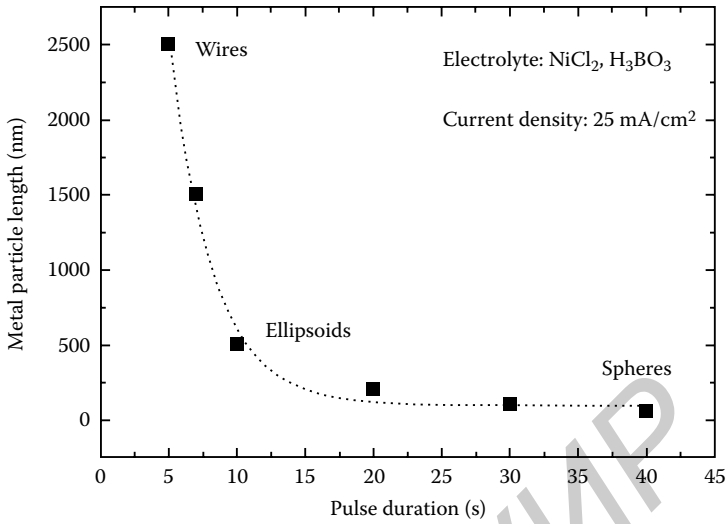

FIGURE 9.2 Relation between pulse duration of current density and elongation of the Ni-structures deposited in the PSi in the same conditions. The length of the Ni structures increases from 60 nm (for sphere-like NPs) to 2.5 μm (for NWs). The diameter of the Ni structures corresponds to pore-diameter, which in average is 60 nm. (From Granitzer P. and Rumpf K., *Materials* 3, 943, 2010. Published by MDPI as open access. With permission.)

weak magnetic fields has been explained by the presence of fine Ni NPs in pores (Granitzer et al. 2006, 2007a,b; Rumpf et al. 2008). Recently, this research group has reported new results on Ni/PSi composites aimed at formation of uniform metal NWs by minimization of roughness of the PSi pore walls. Granitzer et al. (2012) fabricated PSi by anodization with applied external 8 T magnetic field, which was transversely directed to the sample surface and prevented etching of the pore walls. Then Ni was deposited into PSi by the electrochemical method. An enhanced magnetic anisotropy of the final Ni NWs in PSi was demonstrated as shown in Figure 9.3. This practical result is very important for the magnetic memory devices based on Ni NWs formed

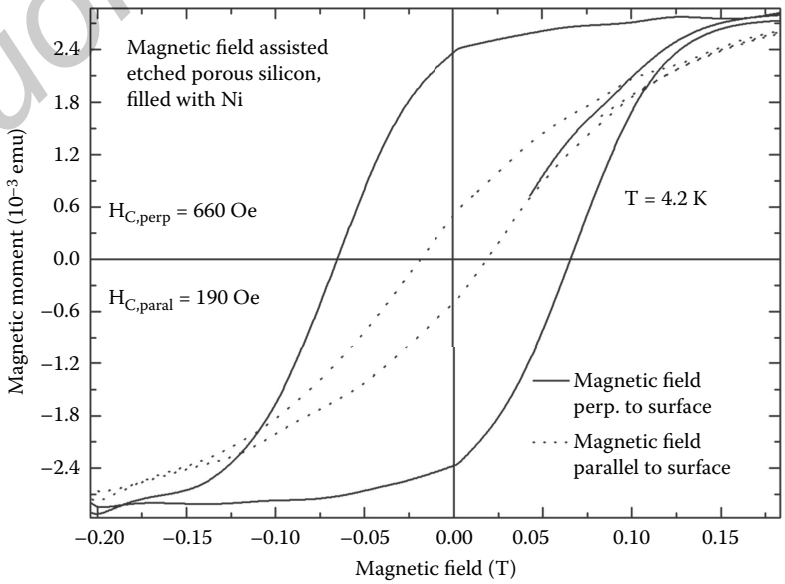

FIGURE 9.3 Magnetic anisotropy observed in a Ni-PS composite for the two magnetization directions parallel (full line) and perpendicular (dotted line) to the Ni nanowires. The PS template was prepared by magnetic anodization. (From from Granitzer P. et al., *Appl. Phys. Lett.* 101, 033110, 2012. Copyright 2012: AIP Publishing. With permission.)

in PSi. The coercivity and remanent magnetization of such structures were studied by Rumpf et al. (2014), which showed that F_f of Ni is 40–50%, and the shape of Ni NWs is defined by the pore channels.

The beneficial influence of smooth pore walls on the coercivity of Ni-filled PSi is demonstrated in Figure 9.4. The results obtained by the research team from the University of Graz are summarized in Granitzer and Rumpf (2010) and Granitzer et al. (2014).

The research group from BSUIR (Dolgiy et al. 2012a,b, 2013) used the galvanostatic electrochemical deposition to deposit Ni in meso-PSi with the fully depleted skeleton with the rough surface. The Ni deposition was shown to start from the NPs formation on endings of the PSi skeleton branches at a depth of 8–10 μm. Then the number of NPs increased in the middle of the PSi layer, and after the prolonged deposition the pores were fully filled with Ni (Figure 9.5).

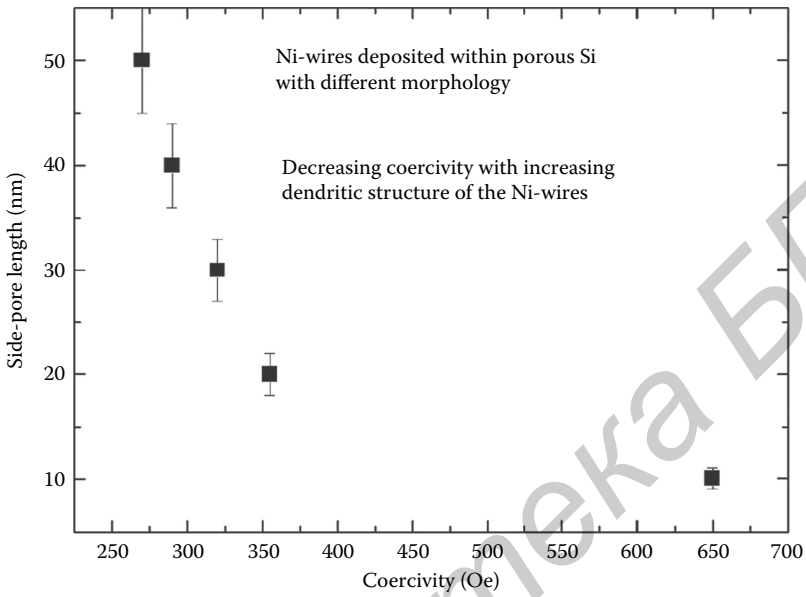

FIGURE 9.4 Coercivity of Ni-filled PSi versus side-pore length of the templates. Decreasing side-pore length is concomitant with an increase of the pore diameter conventionally etched samples. The sample offering a side-pore length of 10 nm has been prepared by magnetic field-assisted etching. (From Rumpf K. et al., *Nanoscale Res. Lett.* 9, 412, 2014. Published by Springer as open access. With permission.)

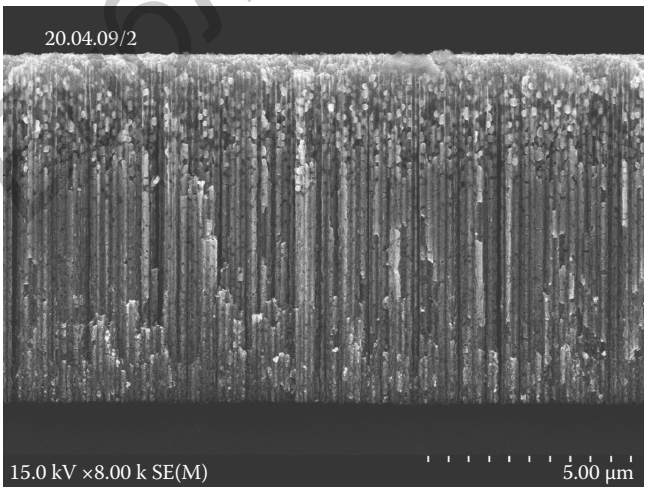

FIGURE 9.5 SEM cross-section image of Ni/PSi composite fabricated by the electrodeposition of Ni into the 10 μm thick and 72% porosity meso-PSi layer.

It was revealed that contact phenomena at the electrolyte/PSi interface play an important role at the electrochemical deposition of Ni in PSi. It happens at the initial stage of the electrochemical process and can lead to the formation of NPs of Ni silicides on the needle parts of the pore walls (Dolgiy et al. 2012b). NPs of Ni silicides are not ferromagnetic; thus, their presence deteriorates magnetic properties of Ni/PSi composite. In such structures, the lattice parameter of Ni was shown to be expanded up to 0.4–0.5% of that of bulk Ni (Prischepa et al. 2014). Magnetic anisotropy of Ni NWs correlated with packing density and pore sizes was found. The dipole interaction was shown to decrease anisotropy and change "easy" axis of magnetization from "along NW" to "perpendicular to NW." The magnetization versus magnetic field measurements for Ni/PSi samples with different deposition time of Ni revealed the dependence of the saturation magnetization value (M_{sat}) on the deposition time (Figure 9.6). It was established that for Ni/PSi samples with longer deposition time starting from 15 min, the specific magnetization is equal to that of bulk Ni (Dolgiy et al. 2013). That moment corresponds to the start of Ni NWs formation in the PSi matrix. Note that the coercivity does not vary significantly with the deposition time.

Michelakaki et al. (2013) from NCSR Demokritos/IMEL compared pulse and galvanostatic regimes at the Ni electrochemical deposition in meso-PSi. The effect of the pulse duration, number of pulses, and total process time on pore filling was investigated for meso-PSi with different porosities and thickness varying in the range of 0.5–4 μm. The authors noticed that the full pore filling and continuous Ni NWs formation are achieved under the galvanostatic electrodeposition, and the results are quite similar to those obtained with the pulsed electrodeposition when the same total deposition time is used in both cases. However, an explanation of the obtained results was not proposed. Probably insensitivity of the Ni deposition to the current density mode is caused by the complete depletion of PSi with charge carriers. Using other electrolytes and PSi of alternative morphology can lead to great variations of the results of the Ni deposition in pulse and constant current density modes. In particular, significant differences may take place at the deposition in thick PSi layers where limited factor is supplying areas of the reduction reaction with the fresh electrolyte. In this case, the impulse mode presents a more effective way of pore filling with Ni.

The electrochemical deposition of Co and Fe in PSi in contrast to the Ni deposition is more compliated. Ronkel et al. (1996) showed that after the potentiostatic Fe deposition into macro-PSi the porous layer is filled with Fe but also contained large amounts of oxygen. The intense SiO_2 formation was supposed to take place while Fe was not oxidized. Renaux et al. (2000) studied the Fe deposition in p^--type PSi. Only the partial pore filling with single Fe clusters was observed. It can be supposed that the Fe deposition in PSi formed on p^--Si should begin on the pore bottoms. Nevertheless, the authors noticed that the Fe deposition occurred simultaneously over all surfaces of the pores.

The electrochemical deposition of alloys of ferromagnetic metals is also possible (Hamadache et al. 2002, 2003). The composition of the deposited Fe-Co varied with the change of ion

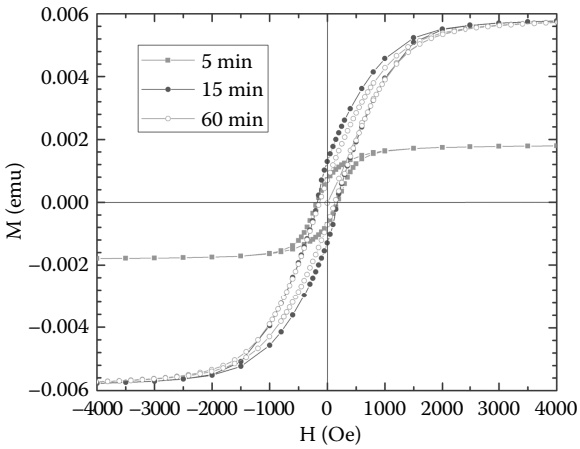

FIGURE 9.6 Magnetization M versus magnetic field H hysteresis loops for PS-Ni samples with different time of Ni deposition. Data are for $T = 5$ K. Magnetic field is oriented parallel to the substrate.

concentrations of these metals in the electrolyte. Pure Co starts depositing from the pore bottoms while the Fe deposition takes place on the pore wall surfaces to give the increased Fe concentration in the upper part of the PSi layer. Increasing Fe ions concentration in the electrolyte caused rising Fe deficiency in the alloy. This was explained by the fact that Co acts as a catalyst for the Fe deposition in the depth of the PSi layer. Even small amounts of Co in the solution (5%) was established to cause the Fe deposition in the whole pore depth rather than at the layer surface. The authors realized good PSi filling with Fe-Co alloys of various percentage compositions. The deposition of the Ni-Fe alloy in PSi by the potentiostatic regime was studied by Ouir et al. (2008). The deposition regimes were shown to influence not only percentage of the alloy composition but also predominant crystallographic orientations of the Ni-Fe compounds. For example, the alloy deposited at 1.25 V consisted of 87% of Ni and 13% of Fe and (111) orientation predominated while the deposition at 1.5 V formed the alloy consisting of 81% of Ni and 19% of Fe and the (111) phase amount was approximately equal to the (220) phase amount.

Co-Pt alloys deposited in PSi (Harraz et al. 2013) also demonstrated magnetic hysteresis when the magnetic field is applied transversely to the sample surface; the coercivity value was equal to 73.13 Oe at that. The sample annealing has resulted in the nearly doubled coercivity and saturation magnetization and the ratio of residual magnetization increased almost an order of magnitude.

Roughness of the PSi pore walls influences magnetic properties of NWs of both pure ferromagnetic metals and alloys. Aravamudhan et al. (2007) fabricated long (up to 100 μm) vertical and branched Ni–Fe nanostructures by the galvanostatic electrochemical deposition in the PSi template. Ni–Fe nanostructures were analyzed for temperature-dependent magnetization and magnetization versus magnetic field measurements. They revealed no magnetic anisotropy of the nanostructures probably due to a balance between "reduced" shape anisotropy from branched and rough pore surfaces and magnetocrystalline anisotropy.

Xu et al. (2007a,b) reported using the displacement deposition method allowing the transformation of the 200-μm thick PSi layer into porous Ni layer. Recently, Zhang et al. (2011) used the displacement method to transform 200-μm thick macro-PSi layer into Ni. The fabricated Ni/PSi composite is shown to be of interest to engineer the Si substrate impedance for microwave crosstalk isolation in mixed-signal integrated circuits (Zhang et al. 2011).

9.2.2 NOBLE METALS

The deposition of noble metals in PSi can be readily made by the displacement method from solutions of metal salts because the standard electrode reduction potential for noble metals in aqueous solutions is positive (Bard et al. 1985). This method has found increasing favor because noble metals are often used as catalysts, so there is no need to form continuous films of these metals.

The Pd deposition by the displacement method is usually carried out from the aqueous or aqueous-alcoholic $PdCl_2$ solutions (Coulthard et al. 1993; Lin et al. 2004; Pedrero et al. 2004). The Pd clusters deposition takes place in the regions of pore entrances and tops of the Si crystallites of PSi. Nevertheless, Razi et al. (2010) showed that very small amounts of metal penetrate into the pores. Large particles of the deposit had the sandwich structure consisting of the first SiO_2 layer, the second Pd_xSi layer, the third pure Pd layer, and the last PdO_2 layer at the particle surface. Prolong stay in air led to increase of the PdO_2 amount while the amount of the pure Pd decreased. The PSi/Pd structures obtained were used as hydrogen sensors allowing detecting hydrogen concentrations up to 0.05–0.17% in dry air.

As Pd, gold is used as a catalyst so Au/PSi composites are important as well. Brito-Neto et al. (2007) have used the displacement method to deposit Au to form a catalytic layer for microfuel cells. The presence of HF in the solution leads to the partial or full dissolution of PSi skeleton during the deposition depending on reactivity of Au containing complexes. The presence of high reactive $[AuCl_4]^-$ complex leads to the complete dissolution of the PSi layer and the chaotic deposition of porous Au in its place. While the displacement method provides the deposition of only a small amount of Au in the pores (Chourou et al. 2011), the electrochemical method allows covering pore walls of macro-PSi with the 100-nm thick Au layer and forming Au microtubes. The decrease of the deposition current density results in the longer deposition time but improves Au film quality.

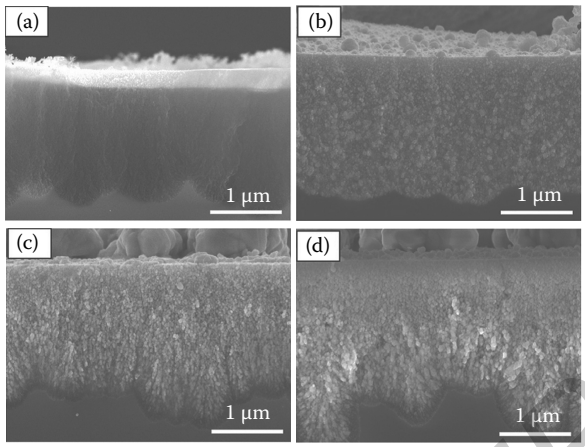

FIGURE 9.7 Cross-sectional SEM of micro-PSi after the electrodeposition of Pt (a, b) and Ag (c, d). The images in (a, c) and (b, d) show the samples of the hydrophilic and hydrophobic PSi, respectively. (From Koda R. et al., *Nanoscale Res. Lett.* 7, 330, 2012. Published by Springer as open access. With permission.)

Other noble metals can be deposited in PSi by the electrochemical method as well. Koda et al. (2012) have deposited Pt and Ag in PSi layers. For the Pt deposition, the deposition behavior was shown to depend on the PSi surface conditions. The deposition in hydrophilic PSi begins from the pore bottoms whereas the Pt deposition in hydrophobic PSi takes place predominantly at the surface. For the Ag deposition, in any case, the deposition begins from the porous layer surface and extends into pore depth independently on the surface type (Figure 9.7). The reason is that at the noble metal deposition in any case the displacement mechanism takes place. For Pt, the displacement is less active in comparison with the electrochemical deposition, and so the process is sensitive to the surface type. For Ag, the deposition by the displacement method predominates and so the surface type influence is insignificant. Moreover, the over voltage at the Pt deposition on the Si electrode is much higher than at the Ag deposition on the Si electrode. Ag does not occlude pore mouths but Pt can occlude them in the case of the hydrophobic surface.

A comparison of Pt, Pd, and Au deposition processes into the ordered macro-PSi of various thicknesses from the solution containing additional amounts of NaCl or Na_2SO_4 was carried out by Fukami et al. (2008). For the Pt and Pd depositions from the solutions containing Na_2SO_4, the deposition has been shown to take place mainly in the pore tops whereas with the NaCl containing solutions the deposition begins from the pore bottoms. For the Au deposition, the attempts to find the regime providing full pore filling with Au have not met with success. With the Na_2SO_4 containing solution, the deposition begins in the pore mouths, and with the NaCl containing solution, the deposition begins from the upper half of the pores and continues to the Au outcropping at the surface. It has been also shown that when deposited in 25-μm thick PSi, the occlusion of pore mouths with Pd deposited occurred in a short time while Pt deposited occluded pore mouths later but pores had not had time to be filled. The Pd deposition in 50-μm thick PSi demonstrated similar behavior while the 50-μm thick PSi layer can be filled with Pt fully. A tenfold decrease in the metal ion concentrations in the solutions has resulted in the Pt spongy deposit and Pd tree-like deposit formation.

9.2.3 CONCLUSIONS

The electrochemical deposition has been used with advantage for the deposition of ferromagnetic metals into PSi. Several teams have already demonstrated Ni NWs in the PSi template with the aspect ratio >1:100 and the filling factor F_f higher than 50%. However, the morphological changes of the pore walls like dendritic branches as well as hydrogen evolution lead to the inhomogeneity of the metal deposit preventing homogeneous filling of the pores. Another problem is related to the exchange of reagents within the pore, which influences the filling factor F_f. If this exchange is

limited, the channels are blocked by the accumulation of the deposited metal. This prevents the uniform filling through the whole length of the pores. From the technological point of view, the pulse mode of the metal electrodeposition seems a more reliable regime to provide uniform pore filling with metals while the galvanostatic regime can be applied for high porosity PSi with the fully depleted skeleton.

For the successful filling of pores with metals by the electrochemical technique, monitoring the potential of the PSi during the electrochemical deposition is of importance to provide *in situ* control of the deposition process stages and to stop the process in the time moments defined by the characteristic points in the potential curve to secure the desired extent of the pore filling with metal. To fabricate cylindrical NWs in the PSi template, the roughness of the PSi pore walls should be minimized. The anodization under the magnetic field action offers a certain scope for that. The pore wall roughness also may be decreased by the use of the pulse modes in the Si anodization as shown by Cheng et al. (2003) and Chubenko et al. (2014). To provide good pore filling with metals, it is very important to provide the full carrier depletion of the PSi skeleton to prevent the current passing through the skeleton and thereby to have the current passing mainly through the pore bottoms, promoting the progressive pore filling with metal from bottoms.

Table 9.1 gives a comprehensive listing of the various metals deposited into PSi and the methods utilized.

9.3 FORMATION, PROPERTIES, AND APPLICATIONS OF SEMICONDUCTOR/PSi COMPOSITES

The deposition of both elementary and compound semiconductors has been made into PSi. The aims of the deposition of elementary Ge and Si were either to form an electric contact to PSi, to create electroluminescent devices, or to obtain SiGe (Halimaoui et al. 1995). The deposition of compound semiconductors mostly presented by II-VI and IV-VI has two goals, which are schematically shown in Figure 9.8. The first one is associated with the formation of the electric contact to PSi layer by the deposition of optically transparent films for the PSi-based electroluminescent optoelectronic devices with the luminescence intensity maximum at 600–900 nm (Hérino et al. 1997). Most compound II-VI and IV-VI semiconductors meet this requirement. The second goal is a creation of composite and a formation of these compounds using PSi as a passive template. Those structures utilize inherent optical properties of II-VI and IV-VI semiconductors since most of them have direct bandgap and high luminescence efficiency (Singh et al. 2007; Balucani et al. 2011).

In most cases, the deposition of elementary and compound semiconductors was carried out in meso-PSi of 70–80% porosity with the thickness not exceeding 1–2 μm. The presence of semiconductors in the PSi pores is usually confirmed by the EDS analysis or Auger electron spectroscopy. SEM images showing actual distribution of deposited semiconductors in the porous layer were not often presented.

9.3.1 II-VI AND IV-VI COMPOUND SEMICONDUCTORS

Dücsö et al. (1996) and Utriainen et al. (1997) made first attempts of the PSi filling with II-VI and IV-VI semiconductors. In their works, the atomic layer deposition (ALD) of the SnO_2 into the PSi layer has been studied. The controlled conformal pore filling of PSi with SnO_2 or SnO_x with the tin concentration gradient across the thickness has been successfully realized by the control of temperature and impulses of the reagent supplying. SnO_2 nanostructures with the aspect ratio 1:140 have been formed. A beneficial effect of deposited SnO_2 coatings on the stability of PSi luminescence and electrical properties was determined.

The research group from the Grenoble University (France) introduced the electrochemical deposition of compound semiconductors in the PSi template from the aqueous solutions. The prime object of their work was the development of transparent conductive electrodes to obtain reliable electric contact to the whole PSi surface including walls and bottom parts of the pores. The electrochemical deposition allows depositing binary compound semiconductors in accordance with the induced codeposition mechanism (Kröger 1978). Montès et al. (1997) made the

TABLE 9.1 Deposition of Metals into PSi Template

Metal	Silicon (Type, Orientation, ρ, Ω·cm)	Deposition Method	Porous Silicon			Result	Application	Ref.
			UIPAC Class	*d*, μm	*P*, %			
Ni	p^+, (100), 0.01	Electrochemical	Meso	10	45	Partial filling	Silicides	Hérino et al. 1985
Ni	p^+, (100), 0.001	Electrochemical	Meso	30	–	Good filling	–	Gusev et al. 1994
Ni	*p*, (100), 1–10	Displacement	Macro	200	–	Transformation of PSi layer into Ni	–	Xu et al. 2007a,b
Ni	n^+, (100), 0.01	Electrochemical, pulse	Meso	10–40	45–80	Ni nanowires and separate particles	Magnetic sensors, magneto-optical and spintronic devices	Rumpf et al. 2006, 2014; Granitzer et al. 2012, 2014
Ni	n^+, (100), 0.01	Electrochemical	Meso	10	72	Ni nanowires; good filling	Magnetic sensors, magneto-optical devices	Dolgiy et al. 2012a,b, 2013
Ni	p^+, (100), 0.001–0.005	Electrochemical, pulse	Meso	1–3	70–88	Ni nanowires; good filling	–	Michelakaki et al. 2013
Co	n^+, (100), 0.01	Electrochemical	Meso	1–5	30–60	Partial filling	Silicides	Borisenko et al. 1989, 1990
Fe	*n*, (111), 4.8–7.1	Electrochemical	Macro	1.5	20–30		Electrical contacts	Ronkel et al. 1996
Fe	p^+, (100)	Electrochemical	Micro	0.3	60–80	Partial filling	–	Renaux et al. 2000
Fe-Co	p^+, (100)	Electrochemical	Micro	0.3	60–80	Good filling	–	Hamadache et al. 2002, 2003
Fe-Ni	*n*, (100), 1–10	Electrochemical	Meso	–	–	Partial filling	–	Ouir et al. 2008
Co-Pt	n^+, (100), 0.01–0.02	Electrochemical	Meso	1	–	Partial filling	–	Harraz et al. 2013
Pd	*p*, (100), 3	Immersion	–	10	–	Clusters	Catalyst	Coulthard et al. 1993
Pd	*p*, (100), 0.6–1	Immersion	–	–	–	Clusters near surface	Gas sensors	Lin et al. 2004
Pd	*p*, (100), 1–5	Immersion	Meso	–	–	Clusters, film on surface	Gas sensors	Pedrero et al. 2004
Pd	*p*, (100)	Immersion	Macro	5	–	Big clusters	Gas sensors	Razi et al. 2010
Au	n^+, (100), 0.007–0.02	Displacement	Meso	10.5	–	Good filling; porous metal	Catalyst layers for micro fuel cells	Brito-Neto et al. 2007
Au	p/p^+, (100), 10–20/0.01–0.02	Displacement, Electrochemical	Macro, Meso	5–50	–	Gold microtubes; different	–	Chourou et al. 2011
Ag, Pt	*p*, (100), 10–20	Electrochemical	–	2, 7	–	Good filling; deposition on surface	–	Koda et al. 2012
Au, Pd, Pt	*p*, (100), 10–20	Electrochemical	Macro	25–100	–	Good filling; partial filling; deposition on surface	–	Fukami et al. 2008

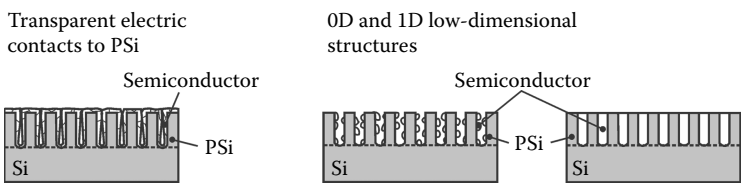

FIGURE 9.8 Major semiconductor/PSi composite strategies of design.

first attempts of the PSi pore filling with CdTe by the electrochemical deposition. CdTe/PSi structures with the CdTe continuous film on the PSi surface were obtained. This approach was also used for the ZnSe deposition (Hérino et al. 1997). However, the conformal pore filling with these materials was not achieved because the deposition of the compounds takes place more intensely at the PSi surface. That problem could be solved by two ways (Montès et al. 2000). The first one is the increase of the electrolyte concentration to increase the ion diffusion rate along the pore channels during the deposition. However, it is complicated for II-VI semiconductors since stochiometric compounds are formed in a limited range of deposition parameters values. The second way is the stimulation of the deposition process in the depth of the pores. It could be done, for example, by substrate illumination with light for which the PSi is transparent and which will be absorbed by the bulk silicon below PSi layer avoiding generation of the excess charge carriers in the top part of the PSi layers. The successful ZnSe deposition into PSi has been made at the continuous illumination of the substrate with 830 nm laser (Montès et al. 2000). As a result, ZnSe was observed only at the bottom part of PSi layer. The tenfold increase of the photoluminescence intensity associated with the defect passivation of the silicon crystallites surface was observed. The thermal annealing of the ZnSe/PSi structures caused the PSi photoluminescence intensity to decrease, red shift of photoluminescence maximum, and improvement of PSi/ZnSe contact electric parameters (Montès et al. 2000; Montès and Hérino 2000).

ZnO can also be deposited in the PSi template by the cathodic electrochemical deposition (Balucani et al. 2011; Chubenko et al. 2011) from the non-aqueous DMSO-based solution. The PSi layer thickness was shown to have significant impact on the ZnO deposition process. At the about 1-μm PSi thickness, the ZnO deposition preferably takes place on the surface of the porous layer; and at the 10-μm PSi layer thickness, the ZnO crystals are formed in the pores to form the composite structure (Figure 9.9). The change in the crystal formation process is associated with an increase in the length and so in the resistance of nanosized crystallites of the PSi skeleton. The structures formed have shown the PL in the visible spectrum range associated with the ZnO crystal lattice defects.

The research of the chemical bath deposition (CBD) of CdS in the PSi layer was made as well (Hérino et al. 1997; Gros-Jean et al. 1998). The deposition was performed from the alkaline cadmium acetate and thioacetamide solutions. With good CdS pore filling, the instability of optical properties of the CdS/PSi composite associated with the Si-H bond breaking at the PSi surface and PSi partial oxidation with the formation of the nonradiation recombination centers has been shown (Gros-Jean et al. 2000). The methyl grafting preceding the CdS deposition allowed the PSi surface to be protected at the CBD of CdS, preventing the PSi luminescence degradation (Gros-Jean et al. 2000).

The ZnSe and CdSe deposition into the PSi template pores can be also fulfilled by the evaporation of metal salts incorporated in PSi followed by selenisation (Belogorokhov et al. 1998, 1999). Obtained composites demonstrated complex PL spectra with bands associated with the emission both from the PSi and from the compound semiconductor clusters in the pores. After the ZnSe and CdSe incorporation into the pores, the PSi emission intensity decreases by 20–50%. Formed

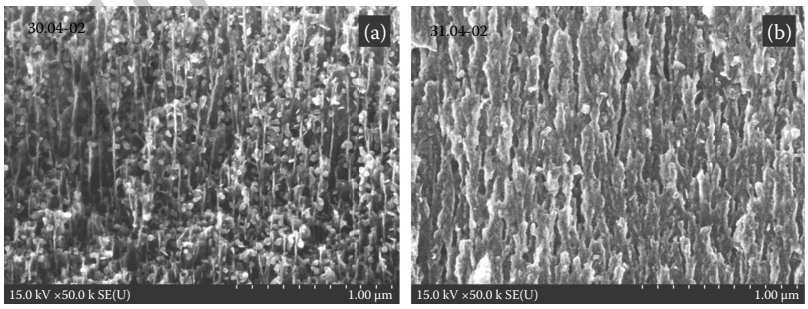

FIGURE 9.9 SEM images of the middle section (depth approximately 3 μm from surface) of meso-PSi layer of 70% porosity with ZnO particles electrochemically deposited from the nonaqueous DMSO based solution: (a) corresponds to shorter deposition time and hence distinct separated ZnO nanocrystals are visible; (b) corresponds to longer deposition time, individual ZnO crystals merged into a continuous film covering the walls of the pores.

film consisted of 3–5 nm sized ZnSe or CdSe quantum dots. A small shift of the photoluminescence maximum positions into the short-wave range relative to these for the bulk crystals of these semiconductors has been observed at that. Non-rectifying CdSe/PSi junction is suitable as the electric contact to the porous layer that is of importance for the PSi-based devices.

Recently the isothermal close space sublimation (ICSS) technique was used for PSi filling with ZnTe and CdSe (Torres-Costa et al. 2012; Melo et al. 2014). Obtained compound semiconductor clusters with polycrystalline structure consisted of crystallites of the stoichiometric or close to stoichiometric composition with the oxygen atom inclusions. The PSi filling has occurred at the whole depth of the PSi layer. The increase of binary semiconductors bandgap caused by quantum-confinement effects has been observed. The self-regulation of the ICSS deposition process due to the equality of substrate and component sources temperature allows a formation of very thin polycrystalline films of compounds in the PSi (Melo et al. 2014).

II-VI and IV-VI oxide semiconductors such as SnO_2 and ZnO can be readily synthesized by the sol-gel deposition. With this technique, sol in the liquid state could penetrate deeply into the pores. However, two conditions should be met at that. The first condition is the assurance of the pore walls wetting with the solution, and the second one is the limitation of the maximum particle size that should not exceed the diameter of PSi pore mouths. For the first time this approach was demonstrated by the example of SnO_2 (Cobianu et al. 1997). Sols used have been prepared on the base of tin ethoxide ethanol solutions. Tin ethoxide based sol has allowed forming SnO_2 in the depth to 1 μm from the PSi layer surface. The sol-gel technique also enables doped SnO_2 films to be formed by the addition of dopant containing additives into the sol (Chatelon et al. 1994). These films doped with Sb or F may be used either as transparent conducting electrodes (Cobianu et al. 1997; Moadhen et al. 2003; Elhouichet et al. 2005; Garcés et al. 2012) or as array that includes optically active particles emitting light in the visible range, for example, rare-earth ions (Elhouichet et al. 2003; Moadhen et al. 2003; Dabboussi et al. 2006). Noteworthy is the SnO_2 films doped with rare-earth ions Eu^{3+} and Tb^{3+} demonstrated optical effects associated with the nonradiative transfer of absorbed optical energy from rare-earth ions to Si crystallites (Elhouichet et al. 2003) or vice versa (Dabboussi et al. 2006). This results in the widening of the absorption spectra of composite material and increasing of the luminescence efficiency.

To form ZnO on the PSi substrates by the sol-gel method, zinc acetate ethanol solutions with the addition of monoethanolamine for the sol stabilization were used (Singh et al. 2007). The composite structures formed have demonstrated a wide emission spectrum in the range of 450–850 nm composed of the PSi (650–850 nm) and ZnO (450–650 nm) emission bands. The ZnO emission is associated with oxygen vacancies and interstitial atoms in the crystal lattice (Singh et al. 2007; Singh et al. 2009a). The healing of defects in the ZnO crystal lattice and at the ZnO/PSi interface allows increasing the luminescence efficiency of composite material (Singh et al. 2009b). Martínez et al. (2014) used the ZnO sol-gel deposition from the same solutions in two-layer PSi for the fabrication of memristive devices. The PSi application has allowed defining formation of ZnO clusters of the required size and increasing the number of oxygen defects in the ZnO crystal lattice responsible for memristive properties of ZnO/PSi structures.

9.3.2 Ge AND Si

The Ge and Si deposition into PSi in the first time was carried out by the chemical vapor deposition in ultra-high vacuum (UHV-CVD) (Halimaoui et al. 1995). For Ge, the full filling of PSi pores has been made at low pressure of $GeH_4 + H_2$ operating gas of 10^{-3} Torr, as revealed by the Ge distribution in depth of the PSi layer. The achieved deposition rate has been 0.01–0.07 nm/min to be two orders lower as compared with the deposition rate on the smooth substrates. At high pressure, the mouth bridging effect has been observed resulting in partial pore filling. For the Si deposition, the effect of pore downsizing in PSi due to the silicon layer formed on the pore walls has been achieved. This result showed promise for obtaining ordered pores of smaller diameter unachievable by conventional anodization methods. However, Halimaoui et al. (1995) have not presented the Ge and Si distribution in pores. Apart from the creation of the Ge electric contact to PSi, the use of PSi as a template for the formation of luminescent Ge clusters was of interest (Liu et al. 1998). The vapor transport deposition method has been used for the Ge deposition in the PSi layer with

13-nm diameter pores. Ge cluster size has been about 5 nm. The Ge clusters showed intense photoluminescence with maximum in the 700-nm range associated with the quantum-sized effects in the Ge clusters and transition of the nonequilibrium carriers generated by radiation from the PSi skeleton into Ge clusters. Unfortunately, the low time stability of the characteristics of the structures obtained that quickly degraded because of gas adsorption from atmosphere should be noted.

The deposition of elementary semiconductors also was made in the composition of more complex compounds intended for "white" light sources. In the work (Abd Rahim et al. 2012), the ability of the ZnO/Ge/PSi structure formation was demonstrated. A sequential deposition of Ge and ZnO has been made by the method of vapor transport deposition in vacuum. As a result, at the least the full filling of pore mouths with materials deposited has been achieved. The structures obtained have shown complex photoluminescence spectra with bands at about 380, 520, and 770 nm associated with the processes of ZnO band-to-band transitions, recombination in nanosize Ge clusters, and defect-related luminescence in ZnO, respectively. Unfortunately, electroluminescent characteristics of Ge/PSi and ZnO/Ge/PSi structures that are critically important for the LED formation on their basis were not shown in the work (Liu et al. 1998; Abd Rahim et al. 2012).

9.3.3 CONCLUSION

The peculiarities of the electrochemical deposition of metals in PSi (Section 9.2.3) are also valid for the electrodeposition of semiconductors in PSi. Nevertheless, it is necessary to note that this method shows worse structural perfection of the deposited semiconductor in contrast to CVD or ALD.

The PSi filling with semiconductor materials to fabricate the electrical contacts for LED did not gain broad development. Composite materials based on PSi, filled with particles of optically active semiconductors, showed the PL spectra covering the wide range of electromagnetic radiation. Interesting effects of nonradiative transfer of energy from Si crystallites to particles of semiconductors and vice versa were observed in a number of experiments. However, LEDs based on such materials have not been presented yet. Use of semiconductor/PSi composite materials to fabricate the heterostructural photodetectors and sensors seems to be more in perspective.

Table 9.2 gives a comprehensive listing of the various compound and elementary semiconductors deposited into PSi and the methods utilized.

9.4 HYBRID MATERIALS FORMED BY INFILTRATION OF PSi WITH ORGANIC SUBSTANCES

There are various options for the formation of hybrid organic-PSi materials. Bonanno and Segal (2011) presented the most obvious possible results (Figure 9.10). Unfortunately, there are no regularities and common approaches to determining the criteria by which one or another option should be used. Each researcher is forced to determine his or her own.

To infiltrate the PSi matrix with polymers, two infiltration procedures can be used. The first infiltration procedure consists of diffusion of the polymers into the pores. Immediately following anodization, a sample is immersed in a polymer solution containing various common organic solvents such as ethanol, acetone, and chloroform. The sample is left in the solution for a specific period of time (from minutes to days) in order to allow the polymers to diffuse into the pores. The diffusion process takes advantage of the highly porous structure of PSi and the created capillary forces. The polymers have a tendency to go into the pores due to the attraction between the porous surface and the polymer solutions. However, this is a slow process because the polymers have large and bulky molecules. In addition, due to the poor solubility of the polymers in the solvents used, the concentration of the solution is dilute.

The second procedure consists of infiltrating the corresponding monomer, as well as radical initiator, into the pores and polymerizing the polymer within the PSi matrix. Similar to the first procedure, capillary forces attract the small organic molecules enabling diffusion into the pores. Since monomers and radical initiators are extremely small when compared to the polymers, infiltration should be more effective.

TABLE 9.2 Deposition of Compound and Elementary Semiconductors into PSi Template

Semiconductor	Silicon (Type, Orientation, ρ, Ω·cm)	Deposition Method	Porous Silicon			Result	Application	Ref.
			UIPAC Class	*d*, μm	*P*, %			
SnO_2	p^+, (100), 0.001	Atomic layer deposition	Meso	2	70	Conformal coverage of pore walls	Gas sensors, optoelectronic devices	Dücsö et al. 1996; Utriainen et al. 1997
SnO_2:Sb	*p*, (100), 8–10	Sol-gel	Meso	2	70–80	SnO_2:Sb penetrate whole porous structure	Transparent electrodes, rectifying contacts to PSi	Elhouichet et al. 2005
SnO_2:F	*p*, (100), 25.5–42.5	Sol-gel	Macro	30	–	Partial penetration of the pores	Transparent electrodes	Garcés et al. 2012
SnO_2:Eu^{3+} SnO_2:Tb^{3+} SnO_2:(Eu^{3+}+ Tb^{3+})	*p*, (100), 8–10	Sol-gel	Meso	2	70	Pore filling	Rare-earth and PSi-based light emitting devices	Elhouichet et al. 2003; Dabboussi et al. 2006
ZnO	*p*, (100), 0.8–1.2	Sol-gel	Meso	–	–	Pore filling with ZnO layer on top	White light luminescence devices	Singh et al. 2007, 2009a,b
ZnO	p^+, (100), 0.002–0.005	Sol-gel	Meso	0,3	–	Pore filling with ZnO layer on top	Memristive devices	Martínez et al. 2014
ZnO	n^+, (100), 0.01	Electro-chemical	Meso	1–10	70	Partial of or full pore filling depending on PS layer thickness	White light luminescence devices	Balucani et al. 2011; Chubenko et al. 2011
ZnSe	*p*, (100), 10	Chemical	Meso	10–15	70	Pores filled with nanometer size clusters	Optoelectronic devices	Belogorokhov et al. 1999
ZnSe	*p*, (100), 8	Electro-chemical	Meso	0.2–2	70	Pores filled with ZnSe from the bottom	Transparent electrodes	Montès et al. 2000
ZnTe	p^+, (100)	Isothermal close space sublimation	Meso	1–1.5	–	Nanocomposite with good pore filling	PSi-based optoelectronic devices	Torres-Costa et al. 2012; Melo et al. 2014
CdSe	*p*, (100), 10	Chemical	Meso	10–15	70	Pores filled with nanometer size clusters	Optoelectronic devices, ohmic contacts	Belogorokhov et al. 1998, 1999
CdSe	p^+, (100)	Isothermal close space sublimation	Meso	1–1.5	–	Nanocomposite with good pore filling	PSi-based optoelectronic devices	Torres-Costa et al. 2012
CdTe	n^+, (100), ≈1	Electro-chemical	Meso	0.1–0.3	70	Partial penetration of the pores	Transparent electrodes	Montès et al. 1997
CdS	*p*, (100), ≈1	Chemical bath deposition	Meso	1	75	Good penetration of the pores	Transparent electrodes	Hérino et al. 1997; Gros-Jean et al. 1998
Si	p^+, (100), 0.01	UHV-CVD	Meso	0.52	80	Full pore filling	Electrical contact to PSi for PSi-based luminescent devices	Halimaoui et al. 1995
Ge	p^+, (100), 0.01	UHV-CVD	Meso	0.52	80	Partial pore filling	Pore dimensions decreasing	Halimaoui et al. 1995
Ge	*p*, (100), 1–3	Thermal evaporation in Ar atmosphere	Meso	–	–	Deposition of 5 nm Ge clusters possibly on pore walls	Ge based light emitting devices	Liu et al. 1998
Ge/ZnO	*n*, (100), 1–10	Thermal evaporation in vacuum	Meso	–	–	Partial pore filling with crystalline Ge and ZnO	PSi/Ge/ZnO based broadband light emitting devices	Abd Rahim et al. 2012

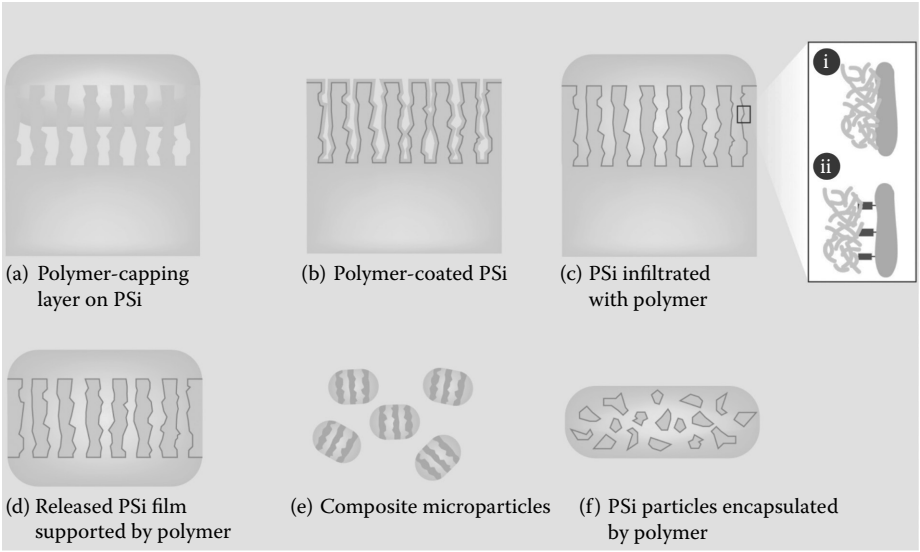

FIGURE 9.10 Strategies for design of polymer/PSi hybrids. (a–f) Depict different formats of hybrid device design as described above each illustration. Inset illustrates interfacial chemistry where polymer is (i) not attached to PSi and (ii) is attached to a chemical modification layer on the surface area of the PSi. Schematics are not drawn to scale. (From Bonanno L.M. and Segal E., *Nanomedicine* 6, 1755, 2011. Copyright 2011: Future Science Group. With permission.)

9.4.1 ORGANIC SUBSTANCES FOR OPTOELECTRONIC DEVICES BASED ON PSi

The scientific community in the 1980s was interested in the possibility of using organic dyes to create tunable lasers in the form of solid-state electronic devices. Canham (1993) used organic dyes: coumarin 47, coumarin 535, fluorescin, rhodamine 6G, and oksazin 750 to improve PSi luminescence. Before an impregnation of PSi with the organic substanses, it was thermally oxidated. Presence of all organic dyes in PSi except fluorescin allowed reaching the effectiveness of the luminescence up to 1%. An increase of the oxidation level of PSi caused rising luminescence effectiveness. Li et al. (1996) studied luminescence kinetics for different dyes introduced into PSi and proposed an idea of energy transfer from PSi exposed with light to dyes' molecules. Letant and Vial (1997) presented a model of the energy exchange between dye molecules and PSi. Several groups (Yin et al. 1998; Gole et al. 1999; Setzu et al. 1999; Li et al. 2000a; Salcedo et al. 2004; Acikgoz et al. 2011) impregnated PSi with different dyes and observed an improvement of the PSi photoluminescence. Pranculis et al. (2013) studied PSi-based nanocomposites with rhodamine and oksazin and proved an ability of the energy exchange between PSi and molecules of dyes. Elhouichet and Oueslati (2001) initiated the thorough works on PSi/dyes nanocomposites. It was shown that the energy transfer from PSi to molecules of dyes actually takes place (Moadhen et al. 2002; Chouket et al. 2007a,b, 2009a,b, 2013; Gelloz et al. 2010). Piryatinski et al. (2007) chose an alternative way. They proposed an introduction of liquid crystals into PSi. It was shown that liquid crystals like other organic substances, interact with PSi promoting the increase of its luminescence. In those days, mechanisms of the interaction of PSi with organic substances were well studied. That allowed the authors to propose a model that explained the results of their experimental work. Later Piryatinski et al. (2010) experimentally demonstrated the improvement of the photoluminescence of PSi caused by the introduction of liquid crystals. Ma et al. (2011) observed that the variation of a number of the liquid crystals introduced into the PSi matrix allows managing a color of PL. Furthermore, they demonstrated a possibility of white light PL.

Along with the research of the fundamental properties of the organic substances/PSi nanocomposites for optical applications works on the development of devices, which can be successfully used in practice, have been conducted. For instance, Lopez et al. (1999) studied the changing PL of PSi. They showed that it is possible not only increase the effectiveness of PL of PSi but also to control PL peak position (Figure 9.11). Guendouz et al. (2003) filled the PSi pores with polymer,

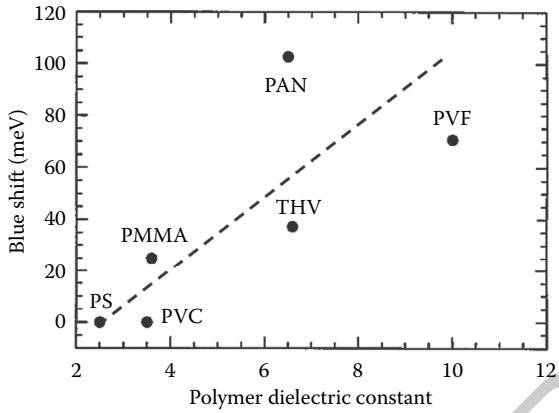

FIGURE 9.11 Photoluminescence blue shift versus polymer dielectric constant at a frequency of 60 Hz. PSi-polymer nanocomposites were produced (74% porosity) by diffusion of the polymers for a period of 2–3 days. Initial peak PL energy before infiltration was 1.63 eV. (From Lopez H.A. et al., *J. Lumin*. 80, 115, 1999. Copyright 1999: Elsevier. With permission.)

which has nonlinear optical properties. Later, they studied the ways of modification of dielectric permittivity of composite while preserving nonlinear optical properties of polymer.

9.4.2 ORGANIC SUBSTANCES FOR PASSIVATION AND FUNCTIONALIZATION OF THE PSi SURFACE

The freshly prepared PSi surface is terminated with hydrogen. Si-H bonds are broken in conditions of atmospheric air (not to mention the more aggressive media) and the surface of the PSi begins adsorbing different atoms and molecules. For this reason, any practical applications deal with passivated PSi. Moreover, for sensors or biomedical devices applications the PSi surface needs to be functionalized. The easiest and most obvious way to passivate the surface—the oxidation of PSi—obviously negates all the qualities inherent to PSi, turning the material into the porous silica. Therefore, the scientific community has taken steps to search for other processing methods of the hydrogenated PSi surface. Lauerhaas et al. (1992) found a high sensitivity of the PSi luminescence to organic substances using solvents. Other parameters of PSi are very sensitive to the organic substances; however, this was revealed later.

Canham (1995) was the first who proposed to use PSi as a bioactive and biocompatible material. Nowadays these peculiar features of PSi have been actively studied. Li et al. (2000b) studied a possibility of using PSi as bioactive material, which delivers Pt-based complex compound into a cancer cell for its destruction. Li et al. (2003) used the PSi as a matrix for the fabrication of the nanostructured polymer biofuntionalized sensors. They underlined the simplicity and accessibility of the process in comparison with nanolithography. Li et al. (2005) proposed a technology to fabricate the photonic crystals based on the nanocomposites polymer/PSi. Stability and high quality of the obtained photonic crystals was denoted. However, no comparison with analogous structures fabricated by other methods has been made.

Chirvony et al. (2006), basing on the formed understanding of the mechanism of the energy interaction of PSi with organic substances, proposed to use porphyrine inbuilt to the PSi matrix as a sensibilizator for the photodynamic therapy of cancer. The function of the sensibilizator is localization in the cancer cells and generation of the singlet oxygen under near IR excitation in the range of transparency of the living cells of the human body.

Sailor research group from University of California actively studies the biomedical application of PSi and reviewed applications of PSi-based composites for the drug delivery into the treating area of the human body at the required time (Anglin et al. 2008). The advantages of PSi biocompatibility and its wide functional possibilities have been demonstrated. Wu et al. (2008) reported about Si microparticles functionalized by hydrosililation and impregnated with drugs toxic for cancer cells. These particles have a controlled delivery rate to the human body. The control is

provided by managing the rate of the composite material oxidation. Further research works on biomedical application of PSi were mostly connected with the use of particles of this porous material (McInnes and Voelcker 2012).

Jane et al. (2009) reviewed the most interesting sensors based on PSi for biomedicine. Various techniques of fabrication of functionalized PSi-based nanocomposites were mentioned as well as registration methods of useful sensors' signal. Bonanno and Segal (2011) presented a review devoted to the biomedical application of hybrid materials polymer/PSi. The review is characterized by a logical systematization of works on the topic and convincible conclusion remarks.

9.4.3 ORGANIC SUBSTANCES FOR ELECTRICAL CONTACTS TO PSi

Since the discovery of the effective visible PL of PSi, the attention of the scientific community has been prevalently directed to the development of the light-emitting devices based on PSi. The greatest expectations have been placed on the use of electroluminescence while it requires electrical injecting contacts. Thermal and magnetron sputtering as well as CVD have not resulted in the fabrication of the electrical contacts to PSi with low resistance and reproducible characteristics. That is why research has turned to the electrochemical methods and organic substances such as polymers.

Matveeva et al. (1993) proposed using conductive polymers (polyaniline, piolifuran, polipirol, polythiophene) as electrical contacts to PSi. Nevertheless, the luminescence has not been studied in the work. One year later, Parkhutik et al. (1994) performed a detailed study of the luminescence of PSi/polyaniline. They investigated the photoluminescence variation in a wide temperature range (from 4 to 300 K). It was found that polyaniline improves the PL of PSi especially in the range of 100–150 K. Koshida et al. (1993) and Li et al. (1994) studied using polyaniline and polipirol for contacting to PSi and showed that the electroluminescence is several times better than in the case of a metallic contact. Halliday et al. (1996) proposed to form the contact and a light-emitting junction simultaneously. In earlier works, polyaniline has been used just as the electrical contact to PSi with the previously formed p-n junction.

Wakefield et al. (1997) made attempts of the fabrication of the effective light emitter based on PSi by using the multilayer heterostructure metal oxide/polymer/PSi. A principle of the method is based on the injection of holes in *n*-type PSi through the conductive polymer. As a result, the quantum effectiveness increased. Furthermore, an operating voltage rose up to 50–60 V.

Kim and Laibinis (1999) proposed a method of the fabrication of a contact polypirole/PSi with more high quality. They used organolithium compound as initial material for forming low-loose polypirole. The resistance of the polypirole contact to PSi was studied in dependence on the pore filling level. It was found that the filling level is influenced by the current density at the polypirole deposition (Moreno et al. 1999).

Antipán Lara and Kathirgamanathan (2000) used polythiophene as a polymer contact to PSi. The final diodes with rectifying contacts emitted white light. Hérino (2000) presented a paper on nanocomposites based on PSi where he reviewed applications of the organic compounds as electrical contacts to PSi and considered the fabrication of the heterostructures organic substances/PSi for the study of some physical phenomenon. There were described known features of the polymer contacts (improved luminescence and pore filling) in comparison to metallic contacts. Disadvantages of the polymer contacts such as high operating voltage, instability, and nonreproducibility were not mentioned in Hérino's review (Hérino et al 1997; Hérino 2000).

Nguyen et al. (2003a,b) developed a modified technology of the PSi filling with polyphenylenevinylene, which provided good filling pores of 10-μm length. The expected improvement of the specific characteristics of the electrical contact was not experimentally proved in the work. The significance of the work is in the finding method of the reversible electrochemical switching studied heterostructure from the conductive to nonconductive state accompanied by changing polymer color. Other polymers such as polyaniline and polythiophene were deposited as electrical contacts to PSi (Harraz 2011). Schultze and Jung (1995) published a paper devoted to the fabrication of heterostructures based on PSi and polymers. It was the first work where PSi was considered as a material-base for the creation of the nanostructured objects (Figure 9.12). There was given a description of the technology and proposed models of the regularities revealed at

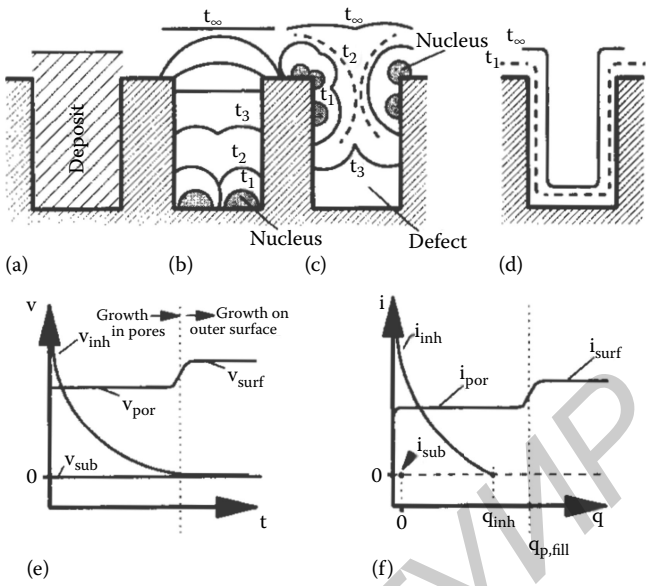

FIGURE 9.12 Mechanistic scheme of pore deposition (a) ideal case; (b) nucleation at the bottoms of the pores; (c) nucleation at the walls of the pores; (d) self inhibiting layer growth; (e) reaction rates v_i versus time t; (f) current density i_j versus charge q. (From Schultze J. and Jung K., *Electrochim. Acta* 40, 1369, 1995. Copyright 1995: Elsevier. With permission.)

the fabrication of the nanosized heterostructures polymer/SiO_2/PSi. The papers on realization of different devices using structure-forming properties of PSi had appeared much later. In 2002, Steinhart et al. (2002) published a short paper on the use of PSi as a matrix-base at fabrication of micro- and nanostructured polymer materials. Their work with more details appeared later (Steinhart et al. 2003, 2004). Although there are many reports on polymer/PSi hybrid fabrication, their application is still unclear (Palacios et al. 2009).

D'arrigo et al. (2003) reported the use of PSi filled with nafiol as a catalytic membrane in miniature fuel cells. It was supposed that the developed specific surface of PSi positively influences specific energy parameters of the final device. Nevertheless, the results of the study of the experimental device were not presented. Mattei and Valentini (2003) proposed their own original method of fabrication of the composite structures based on PSi. The advantage of this method is in simultaneously forming PSi with the required structure and its functionalization. It was realized by the addition of the functionalizing reagents into the solution for the anodization.

9.4.4 CONCLUSIONS

Despite the huge efforts of the scientific community, until now PSi did not become the basis for creating commercial light-emitting devices. Polymer electrical contacts were unreliable and organic dyes did not help. Only a theme of biomedical applications of hybrid organic-PSi materials continues to develop actively. Today appear more and more designs of sensors, therapies, and other practical implementations of useful features of hybrid organic-PSi materials.

9.5 DEPOSITION OF CARBON MATERIALS ON/IN PSi

9.5.1 FULLERENES C60

A growing interest in nanotechnology in general and fullerenes in particular has pushed some research groups to form and study fullerene films on PSi. These works have had just an exploratory character which has not implied solving defined problems. Feng and Miller (1998) used a

method of fixing organic molecules with the fullerene C60 on the surface of PSi by hydrosililation. Photoelectrical and chemical properties of the formed composite material were interesting but not unique. Dattilo et al. (2006) also applied the hydrosililation to fix the molecules of C60 to PSi and studied a wettability of the obtained samples. It was found that the final material demonstrates an increased hydrophoby in comparison to bulk Si. However, the authors noticed that there are alternative chemical compounds, which have much higher hydrophoby on bulk Si and PSi.

9.5.2 CARBON NANOTUBES

Carbon nanotubes (CNTs) are an essential object in nanotechnology. That is why a number of attempts to combine properties of CNTs and PSi have been made to date. Among different features of CNTs the most attention has been paid to the ability of cold emission because this peculiarity is the closest to the luminescent properties of PSi. Fan et al. (1999) reported a fabrication of organized arrays of CNTs on the PSi substrates. According to the proposed model, the main role of PSi is improving ethylene supplying into the growth zone of CNTs. At the same time, CNTs grow on the PSi surface. Later Xu et al. (1999) realized the growth of CNTs directly from the pores of PSi. They showed that dimensions of CNTs depend on a diameter of the pores of the meso- and micro-PSi. The successful results on the cold emission of the formed arrays of CNTs were also reported.

9.5.3 GRAPHITE/GRAPHENE

Carbon in the form of graphite has been applied as an anode of lithium-ion batteries for a long time. It is also known that a theoretical specific energy density (with respect to weight) of the graphite anodes is about one order of magnitude lower than that of Si analogues (370 mA·h/g versus 4200 mA·h/g). However, great variations of the Si anode volume (up to four times) at charge-discharge cycles leading to its fast destruction limit their capabilities. Nevertheless, the specific energy density of Si is so high that research has not left the attempts to fabricate the lithium-ion batteries with the Si-based anode by now. There are also other electrical energy storage graphite-based devices—ionistors or supercapacitors. These devices have electrodes made of graphite with very developed surfaces. Detailed information on PSi-based electrodes of the lithium-ion batteries and supercapacitors is reported in corresponding chapters of this book. Subsections presented next are devoted only to the ways of the PSi/graphite composite fabrication.

An understanding of a shady future of the Si anodes of the lithium-ion batteries led Zheng et al. (2007) to attempt to form carbon-Si composites. Their efforts were directed to the fabrication of composite micro-PSi/graphite/carbon by the mechanochemical reduction for the development of anodes with increased capacity. Specific capacity of the experimental cell was two times more in contrast to commercial lithium-ion batteries. Kim et al. (2008) applied an alternative method of the thermal reduction and formed PSi NPs, which than were passivated by CVD of graphite. As a result, the authors achieved nine times increasing specific capacity of the experimental cells in comparison to commercial analogues. Later, Lv et al. (2009) accurately investigated a synthesis of nanocomposites by the mechanochemical reduction. The authors suggested that precisely developed structure of PSi is responsible for the improved properties of the formed composite. Very recently, Feng et al. (2014) proposed new composite material for the anodes of lithium-ion batteries consisting of micro-PSi, CNTs, and graphite. This composite was fabricated by the magnesium thermal reduction of Si from SiO_2 and following CVD of carbon. The understanding that record levels of Si anodes' capacity has a small presence without evaluating the possibility of their practical application has come soon. The Mg thermal reduction is cheaper than special mills for the fabrication of NPs but still quite expensive for the manufacturing. Jia et al. (2011) used commercially available material SBA-15 as a source for the fabrication of composite anode graphite/PSi. An advantage of the proposed method is an initial structuring SBA-15. Therefore, the production of the anode requires just chemical treating SBA-15. Wang et al. (2012) applied natural diatomite as initial material for the formation of the composite carbon/PSi. Specific capacity

of the experimental cells was four times greater than that of commercial lithium-ion batteries. Moreover, their reliability was higher in comparison to anodes based on SBA-15.

Szczech and Jin (2011) presented a review devoted to research into the application of the nanostructured Si as anodes of lithium-ion batteries. The authors revealed some disadvantages of the performed research such as an absence of a comparison of bulk specific energy densities of the novel and existing anodes. It is connected with the fact that the relation of the stored energy to volume in powerful batteries is more important than the relation of the stored energy to weight. The review ended with the recommendation to use more complex materials for the fabrication of anodes with improved characteristics. Nevertheless, analysis of the composites developed to 2011 has revealed that a main problem preventing their successful practical application is high cost and complexity of the manufacturing. Yin et al. (2012) turned their attention to the problem of Si degradation in composite materials that have been developed for new anode types. An essence of the problem is the presence of fluorine ions in the electrolyte of lithium-ion batteries. An electrolyte aging causes a continuous Si etching.

It has been already mentioned that supercapacitors are devices that are also applied to store electrical energy as lithium-ion batteries. Oakes et al. (2013) reported a supercapacitor based on graphite and PSi. They formed composite material by CVD of graphene-like graphite thin films on PSi. The obtained supercapacitor was compared with the PSi electrode without graphite. An advantage of the composite electrode was obvious while the comparison to other types of supercapacitors was not presented. One year later, Chatterjee et al. (2014) demonstrated the effect of the PSi passivation with graphen to apply it as electrodes of supercapacitors.

9.5.4 CONCLUSIONS

Today, there are two promising applications of hybrid carbon-PSi materials: improved anodes for lithium batteries and electrodes for electrochemical studies. Despite progress in both directions, such materials are still very far from widespread use due to the high cost and complexity of their fabrication.

9.6 SUMMARY

We can now finally summarize that there has been performed a great number of research works on the fabrication and investigation of composite and hybrid materials by the PSi filling with foreign substances. The most remarkable results have been achieved in the deposition of metals from liquids by electrochemical and displacement methods as well as infiltration with polymers. Although, we can expect further research activity on using low cost electrochemical, chemical displacement and infiltration methods, it is clear that an advanced low-temperature CVD and ALD method can provide the highly controlled rate of PSi filling with different foreign substances. These methods also offer a favorable solution for progress on the way from fundamental research to application of composite and hybrid materials based on PSi.

REFERENCES

Abd Rahim, A., Hashim, M., Rusop, M., Ali, N., and Yusuf, R. (2012). Room temperature Ge and ZnO embedded inside porous silicon using conventional methods for photonic application. *Superlattices Microstruct.* **52**, 941–948.

Acikgoz, S., Sarpkaya, I., Milas, P., Inci, M.N., Demirci, G., and Sanyal, R. (2011). Investigation of fluorescence dynamics of BODIPY embedded in porous silicon and monitoring formation of a SiO_2 layer via a confocal FLIM-based NSET method. *J. Phys. Chem. C* **115**, 22186–22190.

Anglin, E.J., Cheng, L., Freeman, W.R., and Sailor, M.J. (2008). Porous silicon in drug delivery devices and materials. *Adv. Drug Delivery Rev.* **60**, 1266–1277.

Antipán Lara, J. and Kathirgamanathan, P. (2000). White light electroluminescence from PSi devices capped with poly (thiophene) as top contact. *Synth. Met.* **110**, 233–240.

Aravamudhan, S., Luongo, K., Poddar, P., Srikanth, H., and Bhansali, S. (2007). Porous silicon templates for electrodeposition of nanostructures. *Appl. Phys. A* **87**, 773–780.

Balucani, M., Nenzi, P., Chubenko, E., Klyshko, A., and Bondarenko, V. (2011). Electrochemical and hydrothermal deposition of ZnO on silicon: From continuous films to nanocrystals. *J. Nanopart. Res.* **13**, 5985–5997.

Bard, A.J., Parsons, R., and Jordan, J. (Eds.) (1985). *Standard Potentials in Aqueous Solution*. Marcel Dekker, New York.

Belogorokhov, A., Belogorokhova, L., Pérez-Rodríguez, A., Morante, J., and Gavrilov, S. (1998). Optical characterization of porous silicon embedded with CdSe nanoparticles. *Appl. Phys. Lett.* **73**, 2766–2768.

Belogorokhov, A., Belogorokhova, L., and Gavrilov, S. (1999). Investigation of properties of porous silicon embedded with ZnSe and CdSe. *J. Cryst. Growth* **197**, 702–706.

Bonanno, L.M. and Segal, E. (2011). Nanostructured porous silicon-polymer-based hybrids: From biosensing to drug delivery. *Nanomedicine* **6**, 1755–1770.

Borisenko, V., Bondarenko, V., and Raiko, V. (1989). Electrochemical deposition of cobalt on porous silicon. *Reports of Academy of Sciences of Belarus Republic* **1**, 528–530.

Borisenko, V., Bondarenko, V., and Raiko, V. (1990). Structure of cobalt disilicides films formed on porous silicon by solid phase reaction. *Rus. J. Surf.: Phys. Chem. Mech.* **4**, 84–90.

Brito-Neto, J.G.A., Kondo, K., and Hayase, M. (2007). Porous gold structures built on silicon substrates. *ECS Trans*. **6**, 223–227.

Canham, L. (1993). Laser dye impregnation of oxidized porous silicon on silicon wafers. *Appl. Phys. Lett.* **63**, 337–339.

Canham, L.T. (1995). Bioactive silicon structure fabrication through nanoetching techniques. *Adv. Mater.* **7**, 1033–1037.

Chatelon, J.P., Terrier, C., Bernstein, E., Berjoan, R., and Roger, J.A. (1994). Morphology of SnO_2 thin films obtained by the sol-gel technique. *Thin Solid Films* **247**, 162–168.

Chatterjee, S., Carter, R., Oakes, L., Erwin, W.R., Bardhan, R., and Pint, C.L. (2014). Electrochemical and corrosion stability of nanostructured silicon by graphene coatings; toward high power porous silicon supercapacitors. *J. Phys. Chem. C* **118**, 10893–10902.

Cheng, X., Feng, Z., and Luo, G. (2003). Effect of potential steps on porous silicon formation. *Electrochim. Acta* **48**, 497–501.

Chirvony, V., Bolotin, V., Matveeva, E., and Parkhutik, V. (2006). Fluorescence and $^1O_2$ generation properties of porphyrin molecules immobilized in oxidized nano-porous silicon matrix. *J. Photochem. Photobiol. A* **181**, 106–113.

Chouket, A., Elhouichet, H., Boukherroub, R., and Oueslati, M. (2007a). Porous silica-laser dye composite: Physical and optical properties. *Phys. Stat. Sol. (a)* **204**, 1518–1522.

Chouket, A., Elhouichet, H., Oueslati, M., Koyama, H., Gelloz, B., and Koshida, N. (2007b). Energy transfer in porous-silicon/laser-dye composite evidenced by polarization memory of photoluminescence. *Appl. Phys. Lett.* **91**, 211902.

Chouket, A., Charrier, J., Elhouichet, H., and Oueslati, M. (2009a). Optical study of planar waveguides based on oxidized porous silicon impregnated with laser dyes. *J. Lumin.* **129**, 461–464.

Chouket, A., Gelloz, B., Koyama, H., Elhouichet, H., Oueslati, M., and Koshida, N. (2009b). Effect of high-pressure water-vapor annealing on energy transfer in dye-impregnated porous silicon. *J. Lumin.* **129**, 1332–1335.

Chouket, A., Cherif, B., Salah, N.B., and Khirouni, K. (2013). Optical and electrical properties of porous silicon impregnated with Congo Red dye. *J. Appl. Phys.* **114**, 243105.

Chourou, M.L., Fukami, K., Sakka, T., and Ogata, Y.H. (2011). Gold electrodeposition into porous silicon: Comparison between meso- and macroporous silicon. *Phys. Status Solidi C* **8**, 1783–1786.

Chubenko, E., Klyshko, A., Bondarenko, V., Balucani, M., Belous, A., and Malyshev, V. (2011). ZnO films and crystals on bulk silicon and SOI wafers: Formation, properties and applications. *Adv. Mater. Res.* **276**, 3–19.

Chubenko, E., Redko, S., Dolgiy, A., and Bondarenko, V. (2014). Fabrication of highly ordered uniform mesoporous silicon for nanocomposite templates. In: *Proc. of E-MRS Fall Meetin*g, Sept. 15–19, 2014, Warsaw, Poland, B11–5.

Cobianu, C., Savaniu, C., Buiu, O. et al. (1997). Tin dioxide sol–gel derived thin films deposited on porous silicon. *Sens. Actuators B* **43**, 114–120.

Coulthard, I., Jiang, D.-T., Lorimer, J.W., Sham, T.K., and Feng, X.-H. (1993). Reductive deposition of Pd on porous silicon from aqueous solutions of $PdCl_2$: An X-ray absorption fine structure study. *Langmuir* **9**, 3441–3445.

D'arrigo, G., Spinella, C., Arena, G., and Lorenti, S. (2003). Fabrication of miniaturised Si-based electrocatalytic membranes. *Mater. Sci. Eng. C* **23**, 13–18.

Dabboussi, S., Elhouichet, H., Ajlani, H., Moadhen, A., Oueslati, M., and Roger, J.A. (2006). Excitation process and photoluminescence properties of Tb^{3+} and Eu^{3+} ions in SnO_2 and in SnO_2: Porous silicon hosts. *J. Lumin.* **121**, 507–516.

Dattilo, D., Armelao, L., Maggini, M., Fois, G., and Mistura, G. (2006). Wetting behavior of porous silicon surfaces functionalized with a fulleropyrrolidine. *Langmuir* **22**, 8764–8769.

Dolgiy, A., Redko, S.V., Bandarenka, H. et al. (2012a). Electrochemical deposition and characterization of Ni in mesoporous silicon. *J. Electrochem. Soc.* **159**, D623–D627.

Dolgiy, A., Bandarenka, H., Prischepa, S. et al. (2012b). Electrochemical deposition of Ni into mesoporous silicon. *ECS Trans*. **41**, 111–118.

Dolgiy, A.L., Redko, S.V., Komissarov, I., Bondarenko, V.P., Yanushkevich, K.I., and Prischepa, S.L. (2013). Structural and magnetic properties of Ni nanowires grown in mesoporous silicon templates. *Thin Solid Films* **543**, 133–137.

Drisko, G.L. and Sanchez, C. (2012). Hybridization in materials science—Evolution, current state, and future aspirations. *Eur. J. Inorg. Chem.* **2012**, 5097–5105.

Dücsö, C., Khanh, N.Q., Horváth, Z. et al. (1996). Deposition of tin oxide into porous silicon by atomic layer epitaxy. *J. Electrochem. Soc*. **143**, 683–687.

Elhouichet, H. and Oueslati, M. (2001). Photoluminescence properties of porous silicon nanocomposites. *Mater. Sci. Eng. B* **79**, 27–30.

Elhouichet, H., Moadhen, A., Férid, M., Oueslati, M., Canut, B., and Roger, J.A. (2003). High luminescent Eu^{3+} and Tb^{3+} doped SnO_2 sol-gel derived films deposited on porous silicon. *Phys. Stat. Sol. (a)* **197**, 350–354.

Elhouichet, H., Moadhen, A., Oueslati, M., Romdhane, S., Roger, J.A., and Bouchriha, H. (2005). Structural, optical and electrical properties of porous silicon impregnated with SnO_2:Sb. *Phys. Stat. Sol. (c)* **2**, 3349–3353.

Fan, S., Chapline, M.G., Franklin, N.R., Tombler, T.W., Cassell, A.M., and Dai, H. (1999). Self-oriented regular arrays of carbon nanotubes and their field emission properties. *Science* **283**, 512–514.

Feng, W. and Miller, B. (1998). Fullerene monolayer-modified porous Si. Synthesis and photoelectrochemistry. *Electrochem. Solid-State Lett*. **1**, 172–174.

Feng, X., Yang, J., Bie, Y., Wang, J., Nuli, Y., and Lu, W. (2014). Nano/micro-structured Si/CNT/C composite from nano-SiO_2 for high power lithium ion batteries. *Nanoscale* **6**, 12532–12539.

Fernández-Pacheco, A., Serrano-Ramón, L., Michalik, J.M. et al. (2013). Three dimensional magnetic nanowires grown by focused electron-beam induced deposition. *Sci. Rep*. **3**, 1492.

Fert, A. and Piraux, L. (1999). Magnetic nanowires. *J. Magn. Magn. Mater*. **200**, 338–358.

Fukami, K., Kobayashi, K., Matsumoto, T., Kawamura, Y.L., Sakka, T., and Ogata, Y.H. (2008). Electrodeposition of noble metals into ordered macropores in p-type silicon. *J. Electrochem. Soc.* **155**, D443–D448.

Garcés, F., Acquaroli, L., Urteaga, R., Dussan, A., Koropecki, R., and Arce, R. (2012). Structural properties of porous silicon/SnO_2:F heterostructures. *Thin Solid Films* **520**, 4254–4258.

Gelloz, B., Harima, N., Koyama, H., Elhouichet, H., and Koshida, N. (2010). Energy transfer from phosphorescent blue-emitting oxidized porous silicon to rhodamine 110. *Appl. Phys. Lett.* **97**, 171107.

Gole, J., DeVincentis, J., and Seals, L. (1999). Optical pumping of dye-complexed and-sensitized porous silicon increasing photoluminescence emission rates. *J. Phys. Chem. B* **103**, 979–987.

Granitzer, P. and Rumpf, K. (2010). Porous silicon—A versatile host material. *Materials* **3**, 943–998.

Granitzer, P., Rumpf, K., Surnev, S., and Krenn, H. (2005). Squid-magnetometry on ferromagnetic Ni-nanowires embedded in oriented porous silicon channels. *J. Magn. Magn. Mater.* **290**–**291**, 735–737.

Granitzer, P., Rumpf, K., and Krenn, H. (2006). Micromagnetics of Ni-nanowires filled in nanochannels of porous silicon. *Thin Solid Films* **515**, 735–738.

Granitzer, P., Rumpf, K., Pölt, P., Reichmann, A., Hofmayer, M., and Krenn, H. (2007a). Magnetization of self-organized Ni-nanowires with peculiar magnetic anisotropy. *J. Magn. Magn. Mater.* **316**, 302–305.

Granitzer, P., Rumpf, K., Pölt, P., Reichmann, A., and Krenn, H. (2007b). Quasi-regular self-organized porous silicon channels metallized with Ni-structures of strong anisotropy. *J. Magn. Magn. Mater.* **310**, e838–e840.

Granitzer, P., Rumpf, K., Ohta, T., Koshida, N., Reissner, M., and Poelt, P. (2012). Enhanced magnetic anisotropy of Ni nanowire arrays fabricated on nano-structured silicon templates. *Appl. Phys. Lett.* **101**, 033110.

Granitzer, P., Rumpf, K., Strzhemechny, Y., and Chapagain, P. (2014). Transient surface photovoltage studies of bare and Ni-filled porous silicon performed in different ambients. *Nanoscale Res. Lett.* **9**, 423.

Grigoras, K., Keskinen, J., Uli-Ranta, E. et al. (2014). ALD modified porous silicon electrodes for supercapacitors. In: *Extended Abstracts of the 9th International Conference on Porous Semiconductors—Science and Technology*, Apr. 9–13, 2014, Alicante-Benidorm, Spain, pp. 314–315.

Gros-Jean, M., Hérino, R., and Lincot, D. (1998). Incorporation of cadmium sulfide into nanoporous silicon by sequential chemical deposition from solution. *J. Electrochem. Soc*. **145**, 2448–2452.

Gros-Jean, M., Hérino, R., Chazalviel, J.-N., Ozanam, F., and Lincot, D. (2000). Formation and characterization of CdS: Methyl-grafted porous silicon junctions. *Mater. Sci. Eng. B* **69**–**70**, 77–80.

Guendouz, M., Pedrono, N., Etesse, R. et al. (2003). Oxidised and non oxidised porous silicon/disperse red 1composite: Physical and optical properties. *Phys. Stat. Sol. (a)* **197**, 414–418.

Gusev, S.A., Korotkova, N.A., Rozenstein, D.B., and Fraerman, A.A. (1994). Ferromagnetic filaments fabrication in porous Si matrix. *J. Appl. Phys*. **76**, 6671–6672.

Halimaoui, A., Campidelli, Y., Badoz, P., and Bensahel, D. (1995). Covering and filling of porous silicon pores with Ge and Si using chemical vapor deposition. *J. Appl. Phys.* **78**, 3428–3430.

Halliday, D., Holland, E., Eggleston, J., Adams, P., Cox, S., and Monkman, A. (1996). Electroluminescence from porous silicon using a conducting polyaniline contact. *Thin Solid Films* **276**, 299–302.
Hamadache, F., Duvial, J.-L., Scheuren, V. et al. (2002). Electrodeposition of Fe–Co alloys into nanoporous p-type silicon: Influence of the electrolyte composition. *J. Mater. Res.* **17**, 1074–1084.
Hamadache, F., Renaux, C., Duvail, J.-L., and Bertrand, P. (2003). Interface investigations of iron and cobalt metallized porous silicon: AES and FTIR analyses. *Phys. Stat. Sol. (a)* **197**, 168–174.
Harraz, F.A. (2011). Impregnation of porous silicon with conducting polymers. *Phys. Stat. Sol. (c)* **8**, 1883–1887.
Harraz, F.A., Tsuboi, T., Sasano, J., Sakka, T., and Ogata, Y.H. (2002). Metal deposition onto a porous silicon layer by immersion plating from aqueous and nonaqueous solutions. *J. Electrochem. Soc.* **149**, C456–C463.
Harraz, F.A., Salem, A.M., Mohamed, B.A., Kandil, A., and Ibrahim, I.A. (2013). Electrochemically deposited cobalt/platinum (Co/Pt) film into porous silicon: Structural investigation and magnetic properties. *Appl. Surf. Sci.* **264**, 391–398.
Hérino, R. (2000). Nanocomposite materials from porous silicon. *Mater. Sci. Eng. B* **69**, 70–76.
Hérino, R., Jan, P., and Bomchil, G. (1985). Nickel plating on porous silicon. *J. Electrochem. Soc*. **132**, 2513–2514.
Hérino, R., Gros-Jean, M., Montès, L., and Lincot, D. (1997). Electrochemical and chemical deposition of II-VI semiconductors in porous silicon. *Mat. Res. Soc. Symp. Proc.* **452**, 467–472.
Jane, A., Dronov, R., Hodges, A., and Voelcker, N.H. (2009). Porous silicon biosensors on the advance. *Trends Biotechnol.* **27**, 230–239.
Jia, H., Gao, P., Yang, J., Wang, J., Nuli, Y., and Yang, Z. (2011). Novel three-dimensional mesoporous silicon for high power lithium-ion battery anode material. *Adv. Energy Mater*. **1**, 1036–1039.
Kim, N.Y. and Laibinis, P.E. (1999). Improved polypyrrole/silicon junctions by surfacial modification of hydrogen-terminated silicon using organolithium reagents. *J. Am. Chem. Soc.* **121**, 7162–7163.
Kim, H., Han, B., Choo, J., and Cho, J. (2008). Three-dimensional porous silicon particles for use in high-performance lithium secondary batteries. *Angew. Chem.* **120**, 10305–10308.
Koda, R., Fukami, K., Sakka, T., and Ogata, Y.H. (2012). Electrodeposition of platinum and silver into chemically-modified microporous silicon electrodes. *Nanoscale Res. Lett*. **7**, 330.
Koshida, N., Koyama, H., Yamamoto, Y., and Collins, G.J. (1993). Visible electroluminescence from porous silicon diodes with an electropolymerized contact. *Appl. Phys. Lett.* **63**, 2655–2657.
Kröger, F. (1978). Cathodic deposition and characterization of metallic or semiconductor binary allows or compounds. *J. Electrochem. Soc*. **125**, 2028–2034.
Labunov, V., Bondarenko, V., Glinenko, L., Dorofeev, A., and Tabulina, L. (1986). Heat treatment effect on porous silicon. *Thin Solid Films* **137**, 123–134.
Lauerhaas, J.M., Credo, G.M., Heinrich, J.L., and Sailor, M.J. (1992). Reversible luminescence quenching of porous silicon by solvents. *J. Am. Chem. Soc.* **114**, 1911–1912.
Letant, S. and Vial, J. (1997). Energy transfer in dye impregnated porous silicon. *J. Appl. Phys.* **82**, 397–401.
Li, K., Diaz, D.C., He, Y., Campbell, J.C., and Tsai, C. (1994). Electroluminescence from porous silicon with conducting polymer film contacts. *Appl. Phys. Lett.* **64**, 2394–2396.
Li, P., Li, Q., Ma, Y., and Fang, R. (1996). Photoluminescence and its decay of the dye/porous-silicon composite system. *J. Appl. Phys*. **80**, 490–493.
Li, H., Xu, D., Guo, G. et al. (2000a). Intense and stable blue-violet emission from porous silicon modified with alkyls. *J. Appl. Phys.* **88**, 4446–4448.
Li, X., John, J.S., Coffer, J.L. et al. (2000b). Porosified silicon wafer structures impregnated with platinum antitumor compounds: Fabrication, characterization, and diffusion studies. *Biomed. Microdev.* **2**, 265–272.
Li, Y.Y., Cunin, F., Link, J.R. et al. (2003). Polymer replicas of photonic porous silicon for sensing and drug delivery applications. *Science* **299**, 2045–2047.
Li, Y.Y., Kollengode, V.S., and Sailor, M.J. (2005). Porous silicon/polymer nanocomposite photonic crystals formed by microdroplet patterning. *Adv. Mater. (Weinheim, Ger.)* **17**, 1249–1251.
Lin, H., Gao, T., Fantini, J., and Sailor, M.J. (2004). A porous silicon-palladium composite film for optical interferometric sensing of hydrogen. *Langmuir* **20**, 5104–5108.
Liu, F.Q., Wang, Z.G., Li, G.H., and Wang, G.H. (1998). Photoluminescence from Ge clusters embedded in porous silicon. *J. Appl. Phys.* **83**, 3435–3437.
Lopez, H.A., Linda Chen, X., Jenekhe, S.A., and Fauchet, P.M. (1999). Tunability of the photoluminescence in porous silicon due to different polymer dielectric environments. *J. Lumin*. **80**, 115–118.
Lv, R., Yang, J., Gao, P., NuLi, Y., and Wang, J. (2009). Electrochemical behavior of nanoporous/nanofibrous Si anode materials prepared by mechanochemical reduction. *J. Alloys Compd.* **490**, 84–87.
Ma, Q., Xiong, R., and Huang, Y.M. (2011). Tunable photoluminescence of porous silicon by liquid crystal infiltration. *J. Lumin.* **131**, 2053–2057.
Martínez, L., Ocampo, O., Kumar, Y., and Agarwal, V. (2014). ZnO-porous silicon nanocomposite for possible memristive device fabsrication. *Nanoscale Res. Lett.* **9**, 437.
Mattei, G. and Valentini, V. (2003). In situ functionalization of porous silicon during the electrochemical formation process in ethanoic hydrofluoric acid solution. *J. Am. Chem. Soc.* **125**, 9608–9609.
Matveeva, E., Parkhutik, V., Diaz Calleja, R., and Martinez-Duart, J. (1993). Growth of polyaniline films on porous silicon layers. *J. Lumin.* **57**, 175–180.

McInnes, S.J., and Voelcker, N.H. (2012). Porous silicon-based nanostructured microparticles as degradable supports for solid-phase synthesis and release of oligonucleotides. *Nanoscale Res. Lett.* **7**(1), 1–10.
Melo, C., Larramendi, S., Torres-Costa, V. et al. (2014). Enhanced ZnTe infiltration in porous silicon by isothermal close space sublimation. *Microporous Mesoporous Mater.* **188**, 93–98.
Michelakaki, E., Valalaki, K., and Nassiopoulou, A.G. (2013). Mesoscopic Ni particles and nanowires by pulsed electrodeposition into porous Si. *J. Nanoparticle Res.* **15**, 1499.
Moadhen, A., Elhouichet, H., and Oueslati, M. (2002). Stokes and anti-stokes photoluminescence of Rhodamine B in porous silicon. *Mater. Sci. Eng. C* **21**, 297–301.
Moadhen, A., Elhouichet, H., Romdhane, S., Oueslati, M., Roger, J.A., and Bouchriha, H. (2003). Structural, optical and electrical properties of SnO_2:Sb:Tb^{3+}/porous silicon devices. *Semicond. Sci. Technol.* **18**, 703–707.
Montès, L. and Hérino, R. (2000). Luminescence and structural properties of porous silicon with ZnSe intimate contact. *Mater. Sci. Eng. B* **69–70**, 136–141.
Montès, L., Muller, F., Gaspard, F., and Hérino, R. (1997). Investigation on the electrochemical deposition of cadmium telluride in porous silicon. *Thin Solid Films* **297**, 35–38.
Montès, L., Muller, F., and Hérino, R. (2000). Localized photo-assisted electro-deposition of zinc selenide into *p*-type porous silicon. *J. Porous Mater.* **7**, 77–80.
Moreno, J., Marcos, M., Agulló-Rueda, F. et al. (1999). A galvanostatic study of the electrodeposition of polypyrrole into porous silicon. *Thin Solid Films* **348**, 152–156.
Nguyen, T., Le Rendu, P., Lakehal, M. et al. (2003a). Filling porous silicon pores with poly (p phenylene vinylene). *Phys. Stat. Sol. (a)* **197**, 232–235.
Nguyen, T.-P., Rendu, P.L., and Cheah, K.W. (2003b). Optical properties of porous silicon/poly (p phenylene vinylene) devices. *Phys. E* **17**, 664–665.
O'Brien, L., Read, D.E., Zeng, H.T., Lewis, E.R., Petit, D., and Cowburn, R.P. (2009). Bidirectional magnetic nanowire shift register. *Appl. Phys. Lett.* **95**, 232502.
Oakes, L., Westover, A., Mares, J.W. et al. (2013). Surface engineered porous silicon for stable, high performance electrochemical supercapacitors. *Sci. Rep.* **3**, 3020.
Ogata, Y., Kobayashi, K., and Motoyama, M. (2006). Electrochemical metal deposition on silicon. *Curr. Opt. Sol. St. Mater. Sci.* **10**, 163–172.
Ouir, S., Sam, S., Fortas, G., Gabouze, N., Beldjilali, K., and Tighilt, F. (2008). FeNi alloys electroplated into porous (*n*-type) silicon. *Phys. Stat. Sol. (c)* **5**, 3694–3697.
Palacios, R., Formentín, P., Santos, A. et al. (2009). Synthesis of ordered polymer micro and nanostructures via porous templates. In: *Proc. of the 2009 Spanish Conference on Electron Devices, CDE 09*, Feb. 11–13, 2009, Santiago de Compostela, Spain, pp. 424–427.
Parbukov, A.N., Beklemyshev, V.I., Gontar, V.M., Makhonin, I.I., Gavrilov, S.A., and Bayliss, S.C. (2001). The production of a novel stain-etched porous silicon, metallization of the porous surface and application in hydrocarbon sensors. *Mater. Sci. Eng. C* **15**, 121–123.
Parkhutik, V., Diaz Calleja, R., Matveeva, E., and Martinez-Duart, J. (1994). Luminescent structures of porous silicon capped by conductive polymers. *Synth. Met.* **67**, 111–114.
Pedrero, L.O., Rena-Sierra, R., and Romero Paredes, G.R. (2004). Gas sensors based on porous silicon and palladium oxide clusters. In: *1st International Conference on Electrical and Electronics Engineering (ICEEE)*, June 24–27, 2004, Acapulco, Mexico, pp. 276–281.
Petrovich, V., Volchek, S., Dolgyi, L. et al. (2000a). Deposition of erbium containing film in porous silicon from ethanol solution of erbium salt. *J. Porous Mater.* **7**, 37–40.
Petrovich, V., Volchek, S., Dolgyi, L. et al. (2000b). Formation features of deposits during a cathode treatment of porous silicon in aqueous solutions of erbium salts. *J. Electrochem. Soc.* **147**, 655–658.
Piryatinski, Y.P., Dolgov, L., Yaroshchuk, O., and Lazarouk, S. (2007). Fluorescence of porous silicon filled with liquid crystal 5CB. *Mol. Cryst. Liq. Cryst.* **467**, 195–202.
Piryatinski, Y.P., Dolgov, L., Yaroshchuk, O., Gavrilko, T., and Lazarouk, S. (2010). Enhancement of fluorescence of porous silicon upon saturation by liquid crystal. *Opt. Spectrosc.* **108**, 70–79.
Pranculis, V., Šimkien, I., Treideris, M., and Gulbinas, V. (2013). Excitation energy transfer in porous silicon/laser dye composites. *Phys. Stat. Sol. (a)* **210**, 2617–2621.
Prischepa, S.L., Dolgiy, A.L., Bandarenka, A.V. et al. (2014). Synthesis and properties of Ni nanowires in porous silicon tempaltes. In: Wilson L.J. (Ed.) *Nanowires: Synthesis, Electrical Properties and Uses in Biological Systems*. Nova Science Publishers, New York, pp. 89–129.
Razi, F., Irajizad, A., and Rahimi, F. (2010). Investigation of hydrogen sensing properties and aging effects of Schottky like Pd/porous Si. *Sens. Actuators B* **146**, 53–60.
Renaux, C., Scheuren, V., and Flandre, D. (2000). New experiments on the electrodeposition of iron in porous silicon. *Microelectron. Reliab.* **40**, 877–879.
Ronkel, F., Schultze, J., and Arens-Fischer, R. (1996). Electrical contact to porous silicon by electrodeposition of iron. *Thin Solid Films* **276**, 40–43.
Rumpf, K., Granitzer, P., Pölt, P., Reichmann, A., and Krenn, H. (2006). Structural and magnetic characterization of Ni-filled porous silicon. *Thin Solid Films* **515**, 716–720.

Rumpf, K., Granitzer, P., and Krenn, H. (2008). Beyond spin-magnetism of magnetic nanowires in porous silicon. *J. Phys. Condens. Matter.* **20**, 454221.
Rumpf, K., Granitzer, P., Koshida, N., Poelt, P., and Reissner, M. (2014). Magnetic interactions between metal nanostructures within porous silicon. *Nanoscale Res. Lett.* **9**, 412.
Salcedo, W.J., Fernandez, F.J., and Rubim, J.C. (2004). Nano-composite of porous silicon and organic dye molecules for optical gas sensor and lasing medium. *Phys. Stat. Sol. (c)* **1**, S26–S30.
Schultze, J. and Jung, K. (1995). Regular nanostructured systems formed electrochemically: Deposition of electroactive polybithiophene into porous silicon. *Electrochim. Acta* **40**, 1369–1383.
Setzu, S., Létant, S., Solsona, P., Romestain, R., and Vial, J. (1999). Improvement of the luminescence in *p*-type as-prepared or dye impregnated porous silicon microcavities. *J. Lumin.* **80**, 129–132.
Singh, R., Singh, F., Agarwal, V., and Mehra, R. (2007). Photoluminescence studies of ZnO/porous silicon nanocomposites. *J. Phys. D: Appl. Phys.* **40**, 3090–3093.
Singh, R., Singh, F., Kanjilal, D., Agarwal, V., and Mehra, R. (2009a). White light emission from chemically synthesized ZnO–porous silicon nanocomposite. *J. Phys. D: Appl. Phys.* **42**, 062002.
Singh, R.G., Singh, F., Sulania, I. et al. (2009b). Electronic excitations induced modifications of structural and optical properties of ZnO-porous silicon nanocomposites. *Nucl. Instrum. Methods Phys. Res., Sect. B* **267**, 2399–2402.
Steinhart, M., Wendorff, J., Greiner, A. et al. (2002). Polymer nanotubes by wetting of ordered porous templates. *Science* **296**, 1997.
Steinhart, M., Wendorff, J., and Wehrspohn, R. (2003). Nanotubes à la carte: Wetting of porous templates. *Chem. Phys. Chem.* **4.11,** 1171–1176.
Steinhart, M., Wehrspohn, R., Gösele, U., and Wendorff, J. (2004). Nanotubes by template wetting: A modular assembly system. *Angew. Chem. Int. Edit.* **43.11**, 1334–1344.
Szczech, J.R. and Jin, S. (2011). Nanostructured silicon for high capacity lithium battery anodes. *Energy Environ. Sci.* **4**, 56–72.
Torres-Costa, V., Melo, C., Climent-Font, A., Argulló-Rueda, F., and Melo, O. (2012). Isothermal close space sublimation for II-VI semiconductor filling of porous matrices. *Nanoscale Res. Lett.* **7**, 409.
Tsuboi, T., Sakka, T., and Ogata, Y.H. (1998). Metal deposition into a porous silicon layer by immersion plating: Influence of halide ions. *J. Appl. Phys.* **83**, 4501–4506.
Utriainen, M., Lehto, S., Niinistö, L. et al. (1997). Porous silicon host matrix for deposition by atomic layer epitaxy. *Thin Solid Films* **297**, 39–42.
Wakefield, G., Dobson, P., Foo, Y., Loni, A., Simons, A., and Hutchison, J. (1997). The fabrication and characterization of nickel oxide films and their application as contacts to polymer/porous silicon electroluminescent devices. *Semicond. Sci. Technol.* **12**, 1304.
Wang, M.-S., Fan, L.-Z., Huang, M., Li, J., and Qu, X. (2012). Conversion of diatomite to porous Si/C composites as promising anode materials for lithium-ion batteries. *J. Power Sources* **219**, 29–35.
Wu, E.C., Park, J.-H., Park, J., Segal, E., Cunin, F., and Sailor, M.J. (2008). Oxidation-triggered release of fluorescent molecules or drugs from mesoporous Si microparticles. *ACS Nano* **2**, 2401–2409.
Xu, D., Guo, G., Gui, L. et al. (1999). Controlling growth and field emission property of aligned carbon nanotubes on porous silicon substrates. *Appl. Phys. Lett.* **75**, 481–483.
Xu, C., Zhang, X., Tu, K.-N., and Xie, Y. (2007a). Nickel displacement deposition of porous silicon with ultrahigh aspect ratio. *J. Electrochem. Soc.* **154**, D170–D174.
Xu, C., Li, M., Zhang, X., Tu, K.-N., and Xie, Y. (2007b). Theoretical studies of displacement deposition of nickel into porous silicon with ultrahigh aspect ratio. *Electrochim. Acta* **52**, 3901–3909.
Yin, F., Xiao, X.R., Li, X.P. et al. (1998). Photoluminescence enhancement of porous silicon by organic cyano compounds. *J. Phys. Chem. B* **102**, 7978–7982.
Yin, Y., Wan, L., and Guo, Y. (2012). Silicon-based nanomaterials for lithium-ion batteries. *Chin. Sci. Bull.* **57**, 4104–4110.
Zhang, X.G. (2001). *Electrochemistry of Silicon and Its Oxide.* Kluwer Academic/Plenum Publishers, New York.
Zhang, X., Xu, C., Chong, K., Tu, K.-N., and Xie, Y.-H. (2011). Study of Ni metallization in macroporous Si using wet chemistry for radio frequency cross-talk isolation in mixed signal integrated circuits. *Materials* **4**, 952–962.
Zheng, Y., Yang, J., Wang, J., and NuLi, Y. (2007). Nano-porous Si/C composites for anode material of lithium-ion batteries. *Electrochim. Acta* **52**, 5863–5867.